

1 **Evaluation of bacterial glycerol dialkyl glycerol tetraether and ^{2}H -
2 ^{18}O biomarker proxies along a Central European topsoil transect**

3 Johannes Hepp^{1,2,*}, Imke K. Schäfer³, Verena Lanny⁴, Jörg Franke³, Marcel
4 Bliedtner^{3,a}, Kazimierz Rozanski⁵, Bruno Glaser², Michael Zech^{2,6}, Timothy I.
5 Eglinton⁴, Roland Zech^{3,a}

6 ¹Chair of Geomorphology and BayCEER, University of Bayreuth, 95440 Bayreuth, Germany and

7 ²Institute of Agronomy and Nutritional Sciences, Soil Biogeochemistry, Martin-Luther-University
8 Halle-Wittenberg, 06120 Halle, Germany

9 ³Institute of Geography and Oeschger Centre for Climate Change Research, University of Bern, 3012
10 Bern, Switzerland

11 ⁴Department of Earth Science, ETH Zurich, 8092 Zurich, Switzerland

12 ⁵Faculty of Physics and Applied Computer Science, AGH University of Science and Technology, 30-
13 059 Kraków, Poland

14 ⁶Institute of Geography, Faculty of Environmental Sciences, Technical University of Dresden, 01062
15 Dresden, Germany

16 ^anow at Institute of Geography, Chair of Physical Geography, Friedrich-Schiller University of Jena,
17 07743 Jena, Germany

18

19 *corresponding author (johannes-hepp@gmx.de)

20 **Keywords**

21 Leaf wax *n*-alkanes, hemicellulose sugars, pH, temperature, CBT, MBT', precipitation $\delta^2\text{H}$ and
22 $\delta^{18}\text{O}$, relative humidity

23 **Abstract**

24 Molecular fossils, like bacterial branched glycerol dialkyl glycerol tetraethers (brGDGTs), and
25 the stable isotopic composition of biomarkers, such as $\delta^2\text{H}$ of leaf wax-derived *n*-alkanes ($\delta^2\text{H}_{n\text{-alkane}}$) or $\delta^{18}\text{O}$ of hemicellulose-derived sugars ($\delta^{18}\text{O}_{\text{sugar}}$) are increasingly used for the
26 reconstruction of past climate and environmental conditions. Plant-derived $\delta^2\text{H}_{n\text{-alkane}}$ and
27 $\delta^{18}\text{O}_{\text{sugar}}$ values record the isotopic composition of plant source water ($\delta^2\text{H}_{\text{source-water}}$ and
28 $\delta^{18}\text{O}_{\text{source-water}}$), which usually reflects mean annual precipitation ($\delta^2\text{H}_{\text{precipitation}}$ and
29 $\delta^{18}\text{O}_{\text{precipitation}}$), modulated by evapotranspirative leaf water enrichment and biosynthetic
30 fractionation. Accuracy and precision of respective proxies should be ideally evaluated at a
31 regional scale. For this study, we analysed topsoils below coniferous and deciduous forests, as
32 well as grassland soils along a Central European transect in order to investigate the variability
33 and robustness of various proxies, and to identify effects related to vegetation. Soil pH-values
34 derived from brGDGTs correlate reasonably well with measured soil pH-values, but
35 systematically overestimate them ($\Delta\text{pH} = 0.6 \pm 0.6$). The branched vs. isoprenoid tetraether
36 index (BIT) can give some indication whether the pH reconstruction is reliable. Temperatures
37 derived from brGDGTs overestimate mean annual air temperatures slightly ($\Delta T_{\text{MA}} = 0.5^\circ\text{C}$
38 ± 2.4). Apparent isotopic fractionation ($\varepsilon_{n\text{-alkane/precipitation}}$ and $\varepsilon_{\text{sugar/precipitation}}$) is lower for
39 grassland sites than for forest sites due to “signal damping”, i.e. grass biomarkers do not record
40 the full evapotranspirative leaf water enrichment. Coupling $\delta^2\text{H}_{n\text{-alkane}}$ with $\delta^{18}\text{O}_{\text{sugar}}$ allows to
41 reconstruct the stable isotopic composition of the source water more accurately than without
42 the coupled approach ($\Delta\delta^2\text{H} = \sim -21\text{‰} \pm 22$ and $\Delta\delta^{18}\text{O} = \sim -2.9\text{‰} \pm 2.8$). Similarly, relative
43 humidity during daytime and vegetation period (RH_{MDV}) can be reconstructed using the coupled
44 isotope approach ($\Delta\text{RH}_{\text{MDV}} = \sim -17 \pm 12$). Especially for coniferous sites, reconstructed RH_{MDV}
45 values as well as source water isotope composition underestimate the measured values. This
46 can be likely explained by understory grass vegetation at the coniferous sites contributing
47 significantly to the *n*-alkane pool but only marginally to the sugar pool in the topsoil. The large
48 uncertainty likely reflect the fact that biosynthetic fractionation is not constant, as well as
49 microclimate variability. Overall, GDGTs and the coupled $\delta^2\text{H}_{n\text{-alkane}}\text{-}\delta^{18}\text{O}_{\text{sugar}}$ approach have
50 great potential for more quantitative paleoclimate reconstructions.

52 1 Introduction

53 Information about the variability and consequences of past climate changes is a prerequisite for
54 precise predictions regarding the present climate change. Molecular fossils, so called
55 biomarkers, have great potential to enhance our understanding about variations of past climate
56 and environmental changes. Lipid biomarkers in particular are increasingly used for
57 paleoclimate and environmental reconstructions (e.g. Brincat et al., 2000; Eglinton and
58 Eglinton, 2008; Rach et al., 2014; Romero-Viana et al., 2012; Schreuder et al., 2016). However
59 strengths and limitations of respective proxies need to be known (Dang et al., 2016). For this,
60 calibrations using modern reference samples are essential.

61 One famous and widely applied lipid biomarker group are terrestrial branched glycerol dialkyl
62 glycerol tetraethers (brGDGTs). They are synthesized in the cell membranes of anaerobe
63 heterotrophic soil bacteria (Oppermann et al., 2010; Weijers et al., 2010) have great potential
64 for the reconstruction of past environmental conditions (e.g. Coffinet et al., 2017; Schreuder et
65 al., 2016; Zech et al., 2012), although some uncertainties exist. Calibration studies suggest that
66 the relative abundance of the individual brGDGTs varies with mean annual air temperature
67 (T_{MA}) and soil pH (Peterse et al., 2012; Weijers et al., 2007), at least across large, global climate
68 gradients or along pronounced altitudinal gradients (Wang et al., 2017). However, in arid
69 regions the production of brGDGT is limited, while isoprenoidal GDGTs (iGDGTs) produced
70 by archaea provide the dominant part of the overall soil GDGT pool (Anderson et al., 2014;
71 Dang et al., 2016; Dirghangi et al., 2013; Wang et al., 2013; Xie et al., 2012). The ratio of
72 brGDGTs vs. isoprenoid GDGTs (BIT) can be used as indication whether a reconstruction of
73 T_{MA} and pH will be reliable. Moreover, Mueller-Niggemann et al. (2016) revealed an influence
74 of the vegetation cover on the brGDGT producing soil microbes. From field experiments, it is
75 known that vegetation type and mulching practice strongly effect soil temperature and moisture
76 (Awe et al., 2015; Liu et al., 2014). Thus, multiple factors can be expected to influence soil
77 microbial communities and GDGT production. So far, little is known about the variability of
78 GDGT proxies on a regional scale, and a calibration study with small climate gradient but with
79 different vegetation types might be useful.

80 Concerning paleohydrology proxies, compound specific stable hydrogen isotopes of leaf wax
81 biomarkers, such as long chain *n*-alkanes ($\delta^2H_{n\text{-alkanes}}$) record the isotopic signal of precipitation
82 and therefore past climate and environmental conditions (Sachse et al., 2004, 2006). However,
83 various influencing factors are known e.g. the moisture source to leaf waxes (Pedentchouk and
84 Zhou, 2018 and Sachse et al., 2012 for review). Next is the evapotranspiration of leaf water
85 (Feehins and Sessions, 2010; Kahmen et al., 2013; Zech et al., 2015), which is strongly driven
86 by relative air humidity (RH; e.g. Cernusak et al., 2016 for review). In addition, a strong
87 precipitation signal is known to be incorporated into long chain leaf waxes (Hou et al., 2008;
88 Rao et al., 2009; Sachse et al., 2004). In paleoclimate studies, it is often not feasible to
89 disentangle between the evapotranspirative enrichment from the precipitation signal. Zech et
90 al. (2013) proposed to couple $\delta^2H_{n\text{-alkane}}$ results with oxygen stable isotopes of hemicellulose-
91 derived sugars ($\delta^{18}O_{\text{sugar}}$). Assuming constant biosynthetic fractionation factors (ε_{bio}) for the
92 different compound classes (*n*-alkanes and hemicellulose sugars), the coupling enables the
93 reconstruction of the isotopic composition of leaf water, RH and δ^2H and $\delta^{18}O$ of plant source
94 water ($\approx \delta^2H$ and $\delta^{18}O$ of precipitation; Tuthorn et al., 2015). So far, a detailed evaluation of

95 this approach on the European scale, as well as related effects concerning vegetation changes
96 is missing.

97 We analysed topsoil samples under coniferous, deciduous and grassland vegetation along a
98 Central European transect in order to estimate the variability of the biomarker proxies. More
99 specifically, we aim to test whether:

100 (i) the vegetation type has an influence on the brGDGT proxies, the $\delta^2\text{H}_{n\text{-alkane}}$ and the $\delta^{18}\text{O}_{\text{sugar}}$
101 stable isotopic composition, as well as on reconstructed $\delta^2\text{H}_{\text{source-water}}$, $\delta^{18}\text{O}_{\text{source-water}}$ and RH.

102 (ii) the published brGDGT proxies used for reconstructing mean annual temperature and soil
103 pH are sensitive enough to reflect the medium changes in temperature and soil pH along our
104 transect.

105 (iii) the coupled $\delta^2\text{H}_{n\text{-alkane}}$ - $\delta^{18}\text{O}_{\text{sugar}}$ approach enables a $\delta^2\text{H}$ and $\delta^{18}\text{O}$ of precipitation and RH
106 reconstruction along the transect.

107

108 **2 Material and methods**

109 **2.1 Geographical setting and sampling**

110 In November 2012, we collected 29 topsoil samples (0-5 cm depth) from 16 locations along a
111 transect from Southern Germany to Southern Sweden (Fig. 1A). We distinguished between sites
112 with coniferous forest (con, n = 9), deciduous forest (dec, n = 14) and grassland (grass, n = 6)
113 vegetation cover (for more details see Schäfer et al. (2016) and Tab. S1).

114

115 **2.2 Database of instrumental climate variables and isotope composition of precipitation**

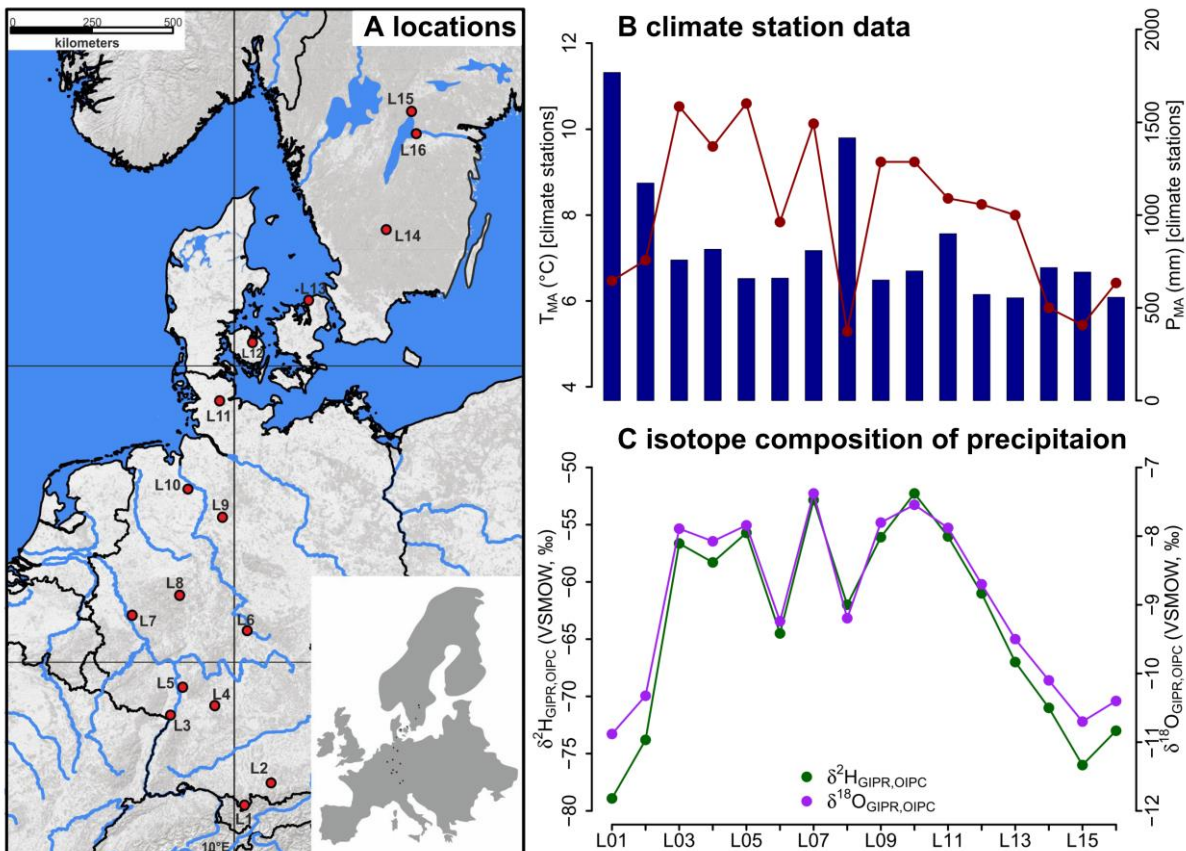
116 Climate data was derived from close-by weather observation stations operating by the regional
117 institutions (Deutscher Wetterdienst (DWD) for Germany, Danmarks Meteorologiske Institut
118 (DMI) for Denmark and the Sveriges Meteorologiska och Hydrologiska Institute (SMHI) for
119 Sweden). The DWD provides hourly data for each station (DWD Climate Data Center, 2018b),
120 enabling not only the calculation of T_{MA} , but also of the mean annual relative air humidity
121 (RH_{MA}), mean temperature and relative air humidity during the vegetation period (T and
122 RH_{MV}), and of daytime temperature and relative humidity averages over the vegetation period
123 (T and RH_{MDV}). In addition, annual precipitation observations were used to derive the mean
124 annual precipitation amount (P_{MA} ; DWD Climate Data Center, 2018b). From the DMI, the
125 respective climate variables were derived from published technical reports (Cappelen, 2002;
126 Frich et al., 1997; Laursen et al., 1999). The SMHI provides open data from which we derived
127 the climate variables for the Swedish sites (Swedish Meteorological and Hydrological Institute,
128 2018). For more details about the climate database used for calculations and comparisons, the
129 reader is referred to Tab. S2.

130 For comprising German precipitation $\delta^2\text{H}/\delta^{18}\text{O}$ along the transect, we realized a regionalisation
131 (called $\delta^2\text{H}_{\text{GIPR}}$ and $\delta^{18}\text{O}_{\text{GIPR}}$) using online available data from 34 German GNIP stations, 4
132 Austrian ANIP stations and the Groningen GNIP station (van Geldern et al., 2014;
133 IAEA/WMO, 2018; Stumpp et al., 2014; Umweltbundesamt GmbH, 2018), following the
134 approach of Schlotter (2007). However, instead of the multivariate regression procedure applied

135 by Schlotter (2007), we used a random forest approach (Hothorn et al., 2006; Strobl et al., 2007,
 136 2008) to describe the relationship of squared latitude, latitude, longitude and altitude vs. long
 137 term weighted means of precipitation $\delta^2\text{H}$ and $\delta^{18}\text{O}$, and realized the prediction for each site
 138 (see supplementary method description for more information). For the Danish and Swedish
 139 sites, such a procedure was not possible. Hence, the annual precipitation $\delta^2\text{H}$ and $\delta^{18}\text{O}$ values
 140 were derived from the Online Isotopes in Precipitation Calculator (OIPC, version 3.1), therefore
 141 called $\delta^2\text{H}_{\text{OIPC}}$ and $\delta^{18}\text{O}_{\text{OIPC}}$ (Bowen, 2018; Bowen and Revenaugh, 2003; IAEA/WMO, 2015).
 142 The finally used $\delta^2\text{H}_{\text{GIPR,OIPC}}$ and $\delta^{18}\text{O}_{\text{GIPR,OIPC}}$ data are given in Tab. S1.

143 The T_{MA} along the transect ranges from 5.3 to 10.6°C, and P_{MA} ranges from 554 to 1769 mm
 144 (Fig. 1B). Precipitation $\delta^2\text{H}/\delta^{18}\text{O}$ shows moderate changes along the transect, $\delta^2\text{H}_{\text{GIPR,OIPC}}$
 145 varies between -52 and -79‰, and $\delta^{18}\text{O}_{\text{GIPR,OIPC}}$ ranges from -7.4 to -10.9‰ (Fig. 1C).

146 Correlations between $\delta^{18}\text{O}_{\text{GIPR,OIPC}}$ and P_{MA} , altitude of the locations, T_{MA} are given in the
 147 supplementary material (Fig. S1 to S3), along with a $\delta^2\text{H}_{\text{GIPR,OIPC}}$ vs. $\delta^{18}\text{O}_{\text{GIPR,OIPC}}$ scatter plot
 148 (Fig. S4).



149
 150 **Fig. 1.** (A) Sample locations (red dots, map source: US National Park Service), (B) variations
 151 of mean annual air temperature (T_{MA} , red dots and line) and mean annual precipitation (P_{MA} ,
 152 blue bars) derived from close-by climate station data, and (C) hydrogen and oxygen stable
 153 isotope composition of precipitation ($\delta^2\text{H}_{\text{GIPR,OIPC}}$ and $\delta^{18}\text{O}_{\text{GIPR,OIPC}}$, respectively) as derived for
 154 the sampled transect locations (see section 2.2 GIPR $\delta^2\text{H}$ and $\delta^{18}\text{O}$ generation procedure). The
 155 reader is referred to section 2.2 (and Tab. S1 and S2) for database and reference information of
 156 data plotted in (B) and (C).

158 **2.3 Soil extractions and analysis**

159 **2.3.1 GDGTs and pH**

160 A detailed description of sample preparation for lipid analysis can be found in Schäfer et al.
161 (2016). Briefly, 1–6 g freeze-dried and grounded soil sample was microwave extracted with 15
162 ml dichloromethane (DCM)/methanol (MeOH) 9:1 (*v*:*v*) at 100°C for 1 h. Extracts were
163 separated over aminopropyl silica gel (Supelco, 45 µm) pipette columns. The nonpolar fraction
164 (including *n*-alkanes) was eluted with hexane and further purified over AgNO₃ coated silica
165 pipette columns (Supelco, 60–200 mesh) and zeolite (Geokleen Ltd.). The GDGT-containing
166 fraction was eluted with DCM:MeOH 1:1 (*v*:*v*), re-dissolved in hexane/isopropanol (IPA) 99:1
167 (*v*:*v*) and transferred over 0.45 µm PTFE filters into 300 µl inserts. For quantification, a known
168 amount of a C₄₆ diol standard was added after transfer. The samples were analysed at ETH
169 Zurich using an Agilent 1260 Infinity series HPLC–atmospheric chemical pressure ionization
170 mass spectrometer (HPLC–APCI-MS) equipped with a Grace Prevail Cyano column (150 mm
171 × 2.1 mm; 3 µm). The GDGTs were eluted isocratically with 90% A and 10% B for 5 min and
172 then with a linear gradient to 18% B for 34 min at 0.2 ml min⁻¹, where A=hexane and
173 B=hexane/isopropanol (9:1, *v*:*v*). Injection volume was 10 µl and single ion monitoring of
174 [M+H]⁺ was used to detect GDGTs.

175 The pH of the samples was measured in the laboratory of the Soil Biogeochemistry group,
176 Institute of Agronomy and Nutritional Sciences, Martin-Luther-University Halle-Wittenberg,
177 using a pH meter in a 1:3 soil:water (*w*:*v*) mixture.

178

179 **2.3.2 δ²H_n-alkane**

180 The hydrogen isotopic composition of the highest concentrated *n*-alkanes (*n*-C₂₅, *n*-C₂₇, *n*-C₂₉,
181 *n*-C₃₁, and *n*-C₃₃) was determined using a TRACE GC Ultra Gas Chromatography connected to
182 a Delta V Plus Isotope Ratio Mass Spectrometer via a ²H pyrolysis reactor kept at 1420 °C (GC-
183 ²H-Py-IRMS; Thermo Scientific, Bremen, Germany) at ETH Zurich (Christoph et al., 2019).
184 For more details about *n*-alkane quantification the reader is referred to Schäfer et al. (2016).
185 The compound-specific ²H/¹H ratios were calibrated against an external standard with C₁₅–C₃₅
186 homologues. External standard mixtures (A4 mix from A. Schimmelmann, University of
187 Indiana) were run between the samples for multipoint linear normalization. The H⁺₃ factor was
188 determined on each measurement day and was constant throughout the periods of the sample
189 batches. Samples were analysed in duplicates, and results typically agreed within 4% (average
190 difference = 1.4%). All δ²H values are expressed relative to the Vienna Standard Mean Ocean
191 Water (V-SMOW).

192

193 **2.3.3 δ¹⁸O_{sugar}**

194 Hemicellulose sugars were extracted and purified using a slightly modified standard procedure
195 (Amelung et al., 1996; Guggenberger et al., 1994; Zech and Glaser, 2009). Briefly, myoinositol
196 was added to the samples prior to extraction as first internal standard. The sugars were released
197 hydrolytically using 4M trifluoroacetic acid for 4 h at 105°C, cleaned over glass fiber filters and
198 further purified using XAD and Dowex columns. Before derivatization with methylboronic acid
199 (Knapp, 1979), the samples were frozen, freeze-dried, and 3-O-methylglucose in dry pyridine

200 was added as second internal standard. Compound-specific hemicellulose sugar ^{18}O
 201 measurements were performed in the laboratory of the Soil Biogeochemistry group, Institute of
 202 Agronomy and Nutritional Sciences, Martin-Luther-University Halle-Wittenberg, using GC-
 203 ^{18}O -Py-IRMS (all devices from Thermo Fisher Scientific, Bremen, Germany). Standard
 204 deviations of the triplicate measurements were 1.4‰ (over 29 investigated samples) for
 205 arabinose and xylose, respectively. We focus on these two hemicellulose-derived neutral sugars
 206 arabinose and xylose as they strongly predominate over fucose in terrestrial plants, soils and
 207 sediments (Hepp et al., 2016 and references therein). Rhamnose concentrations were too low to
 208 obtain reliable $\delta^{18}\text{O}$ results. All $\delta^{18}\text{O}$ values are expressed relative to the Vienna Standard Mean
 209 Ocean Water (V-SMOW).

210

211 **2.4 Theory and Calculations**

212 2.4.1 Calculations used for the GDGT-based reconstructions

213 The branched and isoprenoid tetraether (BIT) index is calculated according to Hopmans et al.
 214 (2004), for structures see Fig. S5:

$$215 \text{BIT} = \frac{\text{Ia+IIa+IIIa}}{\text{Ia+IIa+IIIa+crenarchaeol}}. \quad (1)$$

216 The cyclopentane moiety number of brGDGTs correlates negatively with soil pH (Weijers et
 217 al., 2007), which led to the development of the cyclization of branched tetraethers (CBT) ratio.
 218 CBT and the CBT based pH (pH_{CBT}) were calculated according to Peterse et al. (2012):

$$219 \text{CBT} = -\log \frac{\text{Ib+IIb}}{\text{Ia+IIa}}, \quad (2)$$

$$220 \text{pH}_{\text{CBT}} = 7.9 - 1.97 \times \text{CBT}. \quad (3)$$

221 The number of methyl groups in brGDGTs correlates negatively with T_{MA} and soil pH (Peterse
 222 et al., 2012; Weijers et al., 2007). Thus, the ratio of the methylation of branched tetraethers
 223 (MBT) ratio and the CBT ratio can be used to reconstruct T_{MA} . We use the equation given by
 224 Peterse et al. (2012):

$$225 \text{MBT}' = \frac{\text{Ia+Ib+Ic}}{\text{Ia+Ib+Ic+IIa+IIb+IIc+IIIa}}, \quad (4)$$

$$226 \text{T}_{\text{MA}} = 0.81 - 5.67 \times \text{CBT} + 31.0 \times \text{MBT}'. \quad (5)$$

227

228 2.4.2 Calculations and concepts used for the coupled $\delta^2\text{H}$ - $\delta^{18}\text{O}$ approach

229 The apparent fractionation is calculated according to Cernusak et al. (2016):

$$230 \varepsilon_{n\text{-alkane/precipitation}} = \left(\frac{\delta^2\text{H}_{n\text{-alkane}} - \delta^2\text{H}_{\text{GIPR,OIPC}}}{1 + \delta^2\text{H}_{\text{GIPR,OIPC}}/1000} \right), \quad (6)$$

$$231 \varepsilon_{\text{sugar/precipitation}} = \left(\frac{\delta^{18}\text{O}_{\text{sugar}} - \delta^{18}\text{O}_{\text{GIPR,OIPC}}}{1 + \delta^{18}\text{O}_{\text{GIPR,OIPC}}/1000} \right). \quad (7)$$

232 The isotopic composition of leaf water ($\delta^2\text{H}_{\text{leaf-water}}$ and $\delta^{18}\text{O}_{\text{leaf-water}}$) can be calculated using ε_{bio}
 233 for $\delta^2\text{H}_{n\text{-alkane}}$ (-160‰, Sachse et al., 2012; Sessions et al., 1999) and $\delta^{18}\text{O}_{\text{sugar}}$ (+27‰, Cernusak
 234 et al., 2003; Schmidt et al., 2001):

$$235 \delta^2\text{H}_{\text{leaf-water}} = \left(\frac{1000 + \delta^2\text{H}_{n\text{-alkane}}}{1000 + \varepsilon_{\text{bio}}(n\text{-alkane})} \right) \times 10^3 - 1000, \quad (8)$$

236 $\delta^{18}\text{O}_{\text{leaf-water}} = \left(\frac{1000 + \delta^{18}\text{O}_{\text{sugar}}}{1000 + \varepsilon_{\text{bio}} \text{ (sugar)}} \right) \times 10^3 - 1000.$ (9)

237 Zech et al. (2013) introduced the conceptual model for the coupled $\delta^2\text{H}_{n\text{-alkane}}-\delta^{18}\text{O}_{\text{sugar}}$ approach
 238 in detail. Briefly, the coupled approach is based on the following assumptions (illustrated in
 239 Fig. 8): (i) The isotopic composition of precipitation, which is set to be equal to the plant source
 240 water, typically plots along the global meteoric water line (GMWL; $\delta^2\text{H} = 8 \times \delta^{18}\text{O} + 10$) in a
 241 $\delta^{18}\text{O}$ vs. $\delta^2\text{H}$ space (Craig, 1961); (ii) Source water uptake by plants does not lead to any
 242 fractionation (e.g. Dawson et al., 2002), and significant evaporation of soil water can be
 243 excluded; (iii) Evapotranspiration leads to enrichment of the remaining leaf water along the
 244 local evaporation line (LEL; Allison et al., 1985; Bariac et al., 1994; Walker and Brunel, 1990),
 245 compared to the source water taken up by the plant; (iv) The biosynthetic fractionation is
 246 assumed to be constant. In addition, isotopic equilibrium between plant source water (~
 247 weighted mean annual precipitation) and the local atmospheric water vapour is assumed.
 248 Further assumption concerns the isotope steady-state in the evaporating leaf water reservoir.
 249 The coupled approach allows for reconstructing the isotopic composition of plant source water
 250 ($\delta^2\text{H}_{\text{source-water}}$ and $\delta^{18}\text{O}_{\text{source-water}}$) from the reconstructed leaf water, by calculating the intercepts
 251 of the LELs with the GMWL (Zech et al., 2013). The slope of the LEL (S_{LEL}) can be assessed
 252 by the following equation (Gat, 1971):

253 $S_{\text{LEL}} = \frac{\varepsilon_2^* + C_k^2}{\varepsilon_{18}^* + C_k^{18}},$ (10)

254 where ε^* are equilibrium isotope fractionation factors and C_k are kinetic fractionation factors.
 255 The latter equals to 25.1‰ and 28.5‰, for C_k^2 and C_k^{18} , respectively (Merlivat, 1978). The
 256 equilibrium fractionation factors can be derived from empirical equations (Horita and
 257 Wesolowski, 1994) by using T_{MDV} values. For two Danish sites T_{MDV} are not available, instead
 258 T_{MV} is used here (section 2.2 and Tab. S2).

259 In a $\delta^{18}\text{O}$ - $\delta^2\text{H}$ diagram, the distance of the leaf water from the GMWL define the deuterium-
 260 excess of leaf water ($d_{\text{leaf-water}} = \delta^2\text{H}_{\text{leaf-water}} - 8 \times \delta^{18}\text{O}_{\text{leaf-water}}$, according Dansgaard, (1964); Fig.
 261 8). To convert $d_{\text{leaf-water}}$ into mean RH during daytime and vegetation period (RH_{MDV}), a
 262 simplified Craig-Gordon model can be applied (Zech et al., 2013):

263 $RH = 1 - \frac{\Delta d}{\varepsilon_2^* - 8 \times \varepsilon_{18}^* + C_k^2 - 8 \times C_k^{18}},$ (11)

264 where Δd is the difference in $d_{\text{leaf-water}}$ and the deuterium-excess of source water ($d_{\text{source-water}}$).

265

266 2.5 Statistics

267 In the statistical analysis we checked sample distributions for normality (Shapiro and Wilk,
 268 1965) and for equal variance (Levene, 1960). If normality and equal variances are given, we
 269 perform an Analysis of Variance (ANOVA). If that is not the case, we conduct the non-
 270 parametric Kruskal-Wallis Test. ANOVA or Kruskal-Wallis are used to find significant
 271 differences ($\alpha=0.05$) between the vegetation types (deciduous, conifer and grass).

272 In order to describe the relation along a 1:1 line, the coefficient of correlation (R^2) was
 273 calculated as $R^2 = 1 - \sum (\text{modeled} - \text{measured})^2 / \sum (\text{measured} - \text{measured mean})^2$. The small
 274 r^2 is taken as coefficient of correlation of a linear regression between a dependent (y) and

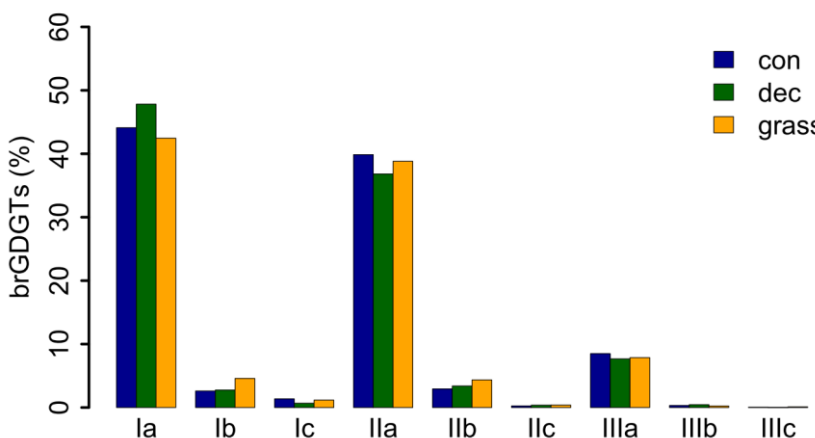
275 explanatory variable(s). The root mean square error (RMSE) of the relationships was calculated
276 as $RMSE = \sqrt{\left(\frac{1}{n} \cdot \sum (\text{modeled} - \text{measured})^2\right)}$. All data plotting and statistical analysis was
277 realized in R (version 3.2.2; R Core Team, 2015).

278

279 **3 Results and Discussion**

280 **3.1 GDGT concentrations**

281 GDGT Ia has the highest concentration under all vegetation types, followed by GDGT IIa and
282 GDGT IIIa (Fig. 2). GDGT Ib, IIb and Ic occur in minor, GDGT IIc and IIIb only in trace
283 amounts. GDGT IIIc was below the detection limit in most of the samples (Tab. S3). Although
284 other studies document an influence of the vegetation cover on soil temperature and soil water
285 content, which control the microbial community composition in soils (Awe et al., 2015; Liu et
286 al., 2014; Mueller-Niggemann et al., 2016), we find no statistically different pattern of the
287 individual brGDGTs.



288

289 **Fig. 2.** Mean concentrations of individual brGDGTs as percentage of all brGDGTs for the three
290 investigated types. Abbreviations: con = coniferous forest sites (n=9); dec = deciduous forest
291 sites (n=14); grass = grassland sites (n=6).

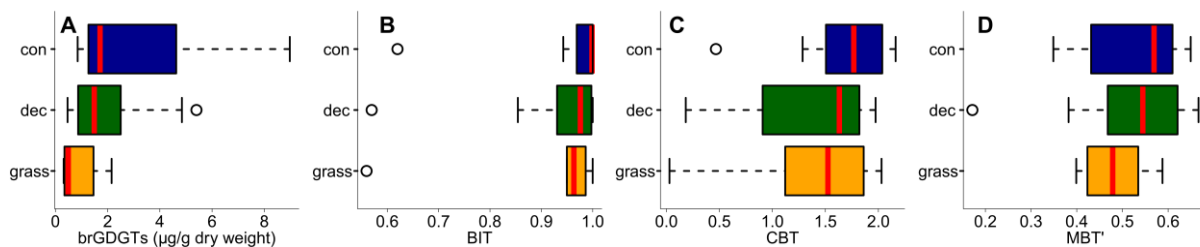
292 Total concentrations of brGDGTs range from 0.32 to 9.17 $\mu\text{g/g}$ dry weight and tend to be
293 highest for the coniferous samples and lowest for the grasses (Fig. 3A, Tab. S3). Bulk brGDGT
294 concentrations lie within the range of other studies examining soils of mid latitude regions
295 (Huguet et al., 2010b, 2010a; Weijers et al., 2011). Similar concentrations in coniferous and
296 deciduous samples imply that brGDGT production does not strongly vary in soils below
297 different forest types. The grass samples show lower brGDGT concentrations compared to the
298 forest samples, but this is probably mainly due to ploughing of the grass sites in former times
299 and hence admixing of mineral subsoil material. The differences in brGDGT concentrations are
300 not significant (p -value = 0.06).

301

302 **3.2 BIT index**

303 Most of the samples have a BIT index higher than 0.9 (Fig 3B and Tab. S3). The BIT-values
304 are typical for soils in humid and temperate climate regions (Weijers et al., 2006). However,

305 outliers exist. The most likely source of iGDGTs in soils are Thaumarchaeota, i.e. aerobic
 306 ammonia oxidizing archaea producing Crenarchaeol and its regioisomer (Schouten et al., 2013
 307 and references therein), precipitation amounts drop below 700-800 mm (Dang et al., 2016;
 308 Dirghangi et al., 2013). The P_{MA} data of our sampling sites mostly show precipitation > 550
 309 mm (Fig. 1B), but one has to be aware that this data is based on the climate station nearest to
 310 the respective sampling locations and microclimate effects, such as sunlight exposure, canopy
 311 cover or exposition might have a pronounced influence on the brGDGT vs. iGDGT distribution.
 312 Mueller-Niggemann et al. (2016) found higher BIT indices in upland soils compared to paddy
 313 soils and stated that the management type also influences BIT values in soils. Along our
 314 transect, grass sites tend to have slightly lower BIT-values than forest sites, probably due to the
 315 absence of a litter layer and hence, no isolation mechanism preventing evaporation of soil water.
 316 Differences between vegetation types are not significant (p-value = 0.32).



317 **Fig. 3.** (A) Total concentrations of brGDGTs in $\mu\text{g g}^{-1}$ dry weight, as well as (B) BIT, (C) CBT
 318 and (D) MBT'. Abbreviations: con = coniferous forest sites (n=9); dec = deciduous forest sites
 319 (n=14); grass = grassland sites (n=6). Box plots show median (red line), interquartile range
 320 (IQR) with upper (75%) and lower (25%) quartiles, lowest whisker still within 1.5IQR of lower
 321 quartile, and highest whisker still within 1.5IQR of upper quartile, dots mark outliers.

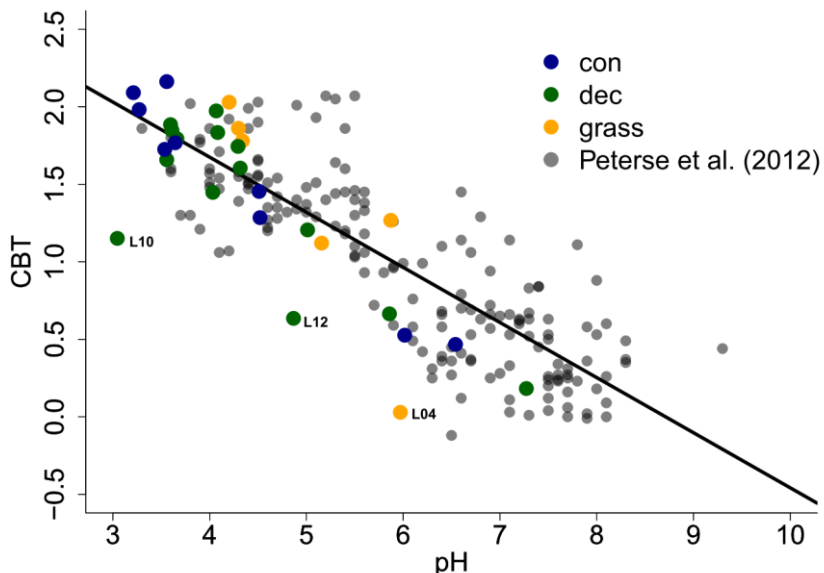
323

324 **3.3 CBT-derived pH**

325 The CBT ratio shows a pronounced variation independent of vegetation type with values
 326 between 0.03 and 2.16 (Fig 3C). The coniferous samples tend to be highest, but the differences
 327 between vegetation types are not significant (p-value = 0.48). The CBT index can be related to
 328 pH in acidic and/or humid soils (e.g. Dirghangi et al., 2013; Mueller-Niggemann et al., 2016;
 329 Peterse et al., 2012; Weijers et al., 2007) but might be an indicator of soil water content and
 330 hence, precipitation in more arid and alkaline soils (e.g. Dang et al., 2016). There is a
 331 pronounced correlation between CBT and soil pH (Fig. 4), which is in good agreement with
 332 other studies from mid latitude regions where precipitation is relatively high (Anderson et al.,
 333 2014 and references therein). Moreover, the CBT to pH relationship in terms of slope and
 334 intersect in our dataset ($\text{CBT} = -0.47 \times \text{pH} + 3.5$, $r^2 = 0.7$, p-value < 0.0001, n = 29) is well
 335 comparable to the correlation described for the global calibration dataset of Peterse et al. (2012)
 336 ($\text{CBT} = -0.36 \times \text{pH} + 3.1$, $r^2 = 0.7$, p-value < 0.0001, n = 176).

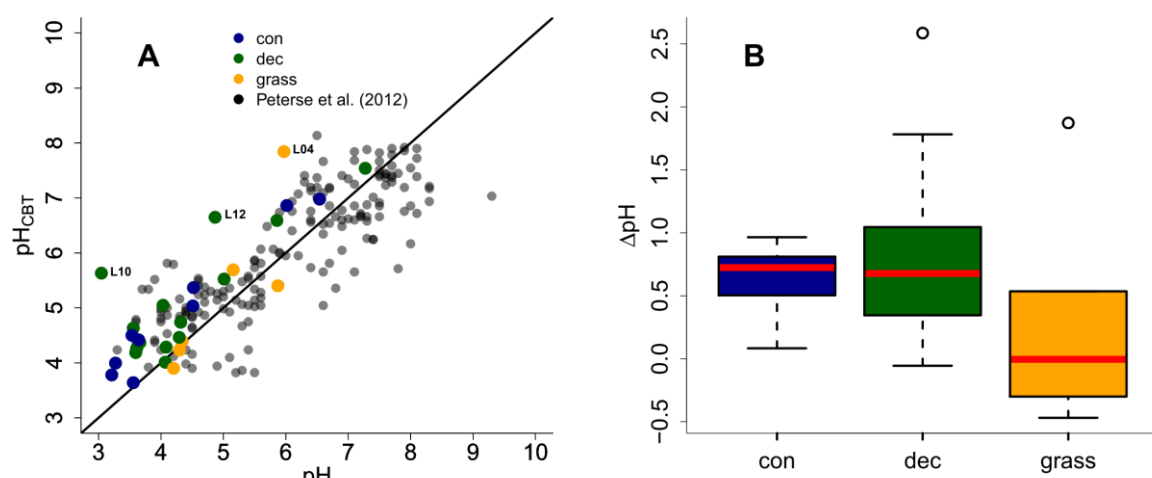
337 However, there are some outliers in the CBT-pH correlation, which need a further examination
 338 (see locations grass L04, dec L10 and dec L12 as marked in Figs. 4 and 5). The outliers show
 339 lower BIT indices (< 0.85, Tab. S3). Even though the data from the nearest climate station
 340 suggest no abnormal P_{MA}. Local effects such as differences in the amount of sunlight exposure,
 341 nutrient availability for brGDGT producing organisms or, most likely soil water content might
 342 influence the brGDGT production at these locations (Anderson et al., 2014; Dang et al., 2016).

343 A lower BIT index as well as a lower CBT occur when soil water content decreases (Dang et
 344 al., 2016; Sun et al., 2016) or when aeration is high and less anoxic microhabitats for GDGT
 345 producing microbes exist (e.g. Dirghangi et al., 2013).



346
 347 **Fig. 4.** CBT to pH relationship in our dataset in comparison to the global calibration dataset
 348 from Peterse et al. (2012) ($CBT = -0.36 \times pH + 3.1$, $r^2 = 0.7$, p-value < 0.0001, n = 176, black
 349 line). Abbreviations: con = coniferous forest sites (n=9); dec = deciduous forest sites (n=14);
 350 grass = grassland sites (n=6).

351
 352 As the CBT and pH are similarly correlated in our dataset and the global dataset of Peterse et
 353 al. (2012), the CBT-derived pH correlated well with the actual pH (Fig. 5A; $R^2 = 0.3$).
 354 Expressed as ΔpH (CBT-derived pH - measured pH), there is a tendency that the GDGTs result
 355 in an overestimation of the real pH for the forest sites (Fig. B). Yet a Kruskal-Wallis test shows
 356 no statistically significant difference between the vegetation types, with a p-value of 0.13. The
 357 overall ΔpH of 0.6 ± 0.6 shows that the reconstruction of soil pH using brGDGTs works well
 358 along this transect.



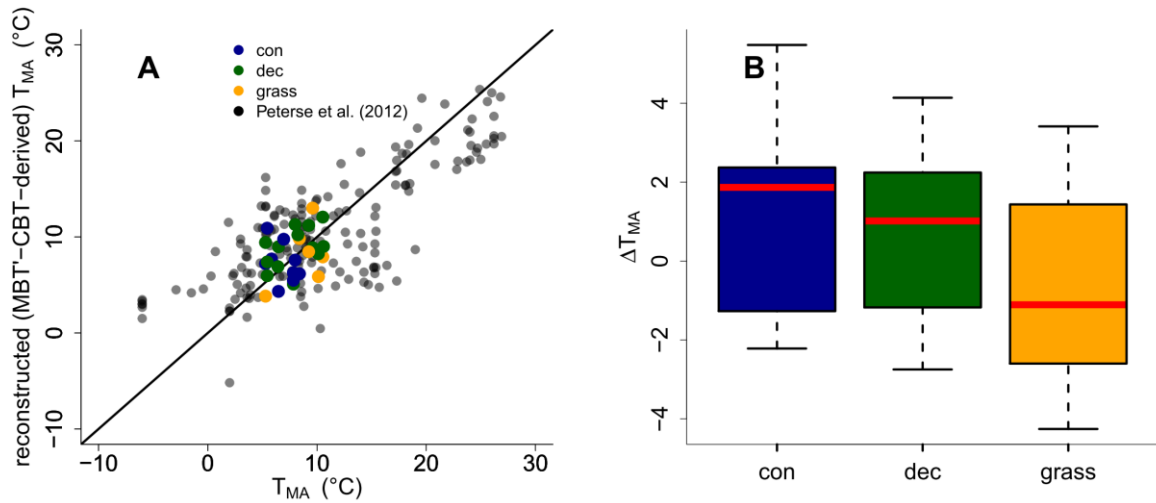
359

360 **Fig. 5.** (A) Correlation between measured pH and reconstructed soil pH (pH_{CBT}) from our
 361 transect data in comparison to the global calibration dataset from Peterse et al. (2012) ($R^2 = 0.7$,
 362 RMSE = 0.75, $n = 176$). Black line indicates the 1:1 relationship. (B) Boxplots of ΔpH (refers
 363 to $\text{pH}_{\text{CBT}} - \text{pH}$). Box plots show median (red line), interquartile range (IQR) with upper (75%)
 364 and lower (25%) quartiles, lowest whisker still within 1.5IQR of lower quartile, and highest
 365 whisker still within 1.5IQR of upper quartile, dots mark outliers. Abbreviations: con =
 366 coniferous forest sites ($n=9$); dec = deciduous forest sites ($n=14$); grass = grassland sites ($n=6$).

367

368 **3.4 MBT'-CBT-derived T_{MA} reconstructions**

369 The MBT' shows high variability with values ranging from 0.17 to 0.67 no statistical
 370 differences between vegetation types ($p\text{-value} = 0.54$; Fig. 3D, Tab. S3). When comparing
 371 reconstructed (MBT'-CBT-derived) T_{MA} with climate station T_{MA} , the data plot close to the 1:1
 372 line, and fit well into the global dataset of Peterse et al. (2012) (Fig. 6A). The ΔT_{MA} reveal an
 373 overall offset of $0.5^{\circ}\text{C} \pm 2.4$ and there is no statistically difference between vegetation types
 374 (Fig. 6B). The standard deviation in ΔT_{MA} of ± 2.4 is well in line with the RMSE of 5.0 for the
 375 global calibration dataset (Peterse et al., 2012).



376

377 **Fig. 6.** (A) Correlation between climate station T_{MA} and reconstructed (MBT'-CBT-derived)
 378 T_{MA} . For comparison, the global calibration dataset from Peterse et al. (2012) is shown. The
 379 black line indicates the 1:1 relationship. (B) Boxplots of ΔT_{MA} (refers to reconstructed T_{MA} -
 380 T_{MA} from climate stations) in the different vegetation types from our transect study. Box plots
 381 show median (red line), interquartile range (IQR) with upper (75%) and lower (25%) quartiles,
 382 lowest whisker still within 1.5IQR of lower quartile, and highest whisker still within 1.5IQR of
 383 upper quartile, dots mark outliers. Abbreviations: con = coniferous forest sites ($n=9$); dec =
 384 deciduous forest sites ($n=14$); grass = grassland sites ($n=6$).

385

386 **3.5 Potential impact of the used liquid chromatography method on pH and T_{MA} reconstructions**

388 The GDGT data presented in this study are not acquired on the up-to-date method (e.g. compare
 389 De Jonge et al., 2014 vs. Zech et al., 2012c). De Jonge et al. (2014) presented a new liquid
 390 chromatography method which enables the separation for the brGDGTs with m/z 1036, 1034

391 and 1032, 1050, 1048 and 1046 into 6-methyl and 5-methyl stereoisomers. The old method did
392 not allow such a separation (Zech et al., 2012c), thus in the calibration often the sum of 6 and
393 5-methylated brGDGTs was used (see and compare De Jonge et al., 2014 vs. Peterse et al., 2012).
394 This introduce scatter to the MBT'-CBT-based T_{MA} reconstructions and can cause a correlation
395 between pH and MBT' (for more details see De Jonge et al., 2014). De Jonge et al. (2014)
396 moreover show that the 6-methyl brGDGTs are ubiquitous abundant in soils from all over the
397 world, based on reanalysing the dataset of Peterse et al. (2012). However, they also compare
398 reconstructed T_{MA} values based MBT'-CBT calibration (Peterse et al., 2012) and their new
399 developed T_{MA} calibration and state that they plot around a 1:1 line. They furthermore state,
400 that especially for arid areas larger deviations can be expected. Finally, they conclude that the
401 use of the new developed calibrations will improve the T_{MA} and pH reconstructions for areas
402 with arid climate conditions. Because our study transect spans from southern Germany to
403 southern Sweden, representing temperate and humid climate conditions, we argue that the usage
404 of the older liquid chromatography method do not introduce a systematic error in our T_{MA} and
405 pH reconstructions. Still, a higher variability/scatter could be associated with the calibration of
406 Peterse et al. (2012) and therefore also present in our T_{MA} and pH reconstructions.

407

408 **3.6 Apparent fractionation of δ^2H and $\delta^{18}O$ in the different vegetation types**

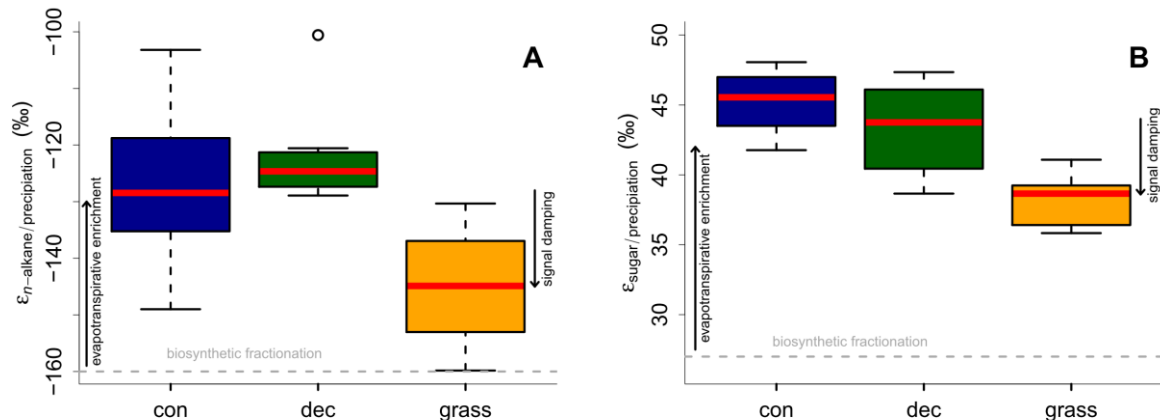
409 The δ^2H values could be obtained for *n*-alkanes C₂₇, C₂₉ and C₃₁ in all samples and additionally
410 at two locations for *n*-C₂₅ and *n*-C₃₃ at six other locations. The $\delta^2H_{n\text{-alkane}}$ values, calculated as
411 mean of *n*-C₂₅ to *n*-C₃₁ δ^2H , ranges from -156 to -216‰. Pooled standard deviations show an
412 overall average of 3.6‰. The $\delta^{18}O_{\text{sugar}}$ values, calculated as the area weighted means for
413 arabinose and xylose, ranges from 27.7 to 39.4‰. The average weighted mean standard
414 deviation is 1.4‰. The compound-specific isotope data is summarized along with the
415 calculations in Tab. S4.

416 Apparent fractionation ($\varepsilon_{n\text{-alkane/precipitation}}$) is on the order of -120 to -150‰, i.e. a bit less than
417 the biosynthetic fraction of -160‰. This implies that evapotranspirative enrichment is ~ 10 to
418 40‰ (Fig. 7A). $\varepsilon_{n\text{-alkane/precipitation}}$ is lower for grass sites compared to the forest sites. Differences
419 are significant between deciduous and grass sites (p-value = 0.005). This finding supports the
420 results of other studies (Kahmen et al., 2013; Liu and Yang, 2008; McInerney et al., 2011), and
421 can be named “signal damping”. Grasses do not only incorporate the evaporatively-enriched
422 leaf water only but also unenriched xylem water in the growth and differentiation zone of
423 grasses (Gamarra et al., 2016; Liu et al., 2017).

424 The grass-derived hemicellulose sugar biomarkers do not fully record the evapotranspirative
425 enrichment of the leaf water, either, as indicated by lower apparent fractionation ($\varepsilon_{\text{sugar/precipitation}}$)
426 in Fig. 7B. The differences are significant between forest and grass sites (p-value < 0.005). This
427 is in agreement with a study on cellulose extracted from grass blades (Helliker and Ehleringer,
428 2002), and again, the “signal damping” can be explained with incorporation of enriched leaf
429 water and non-enriched stem water.

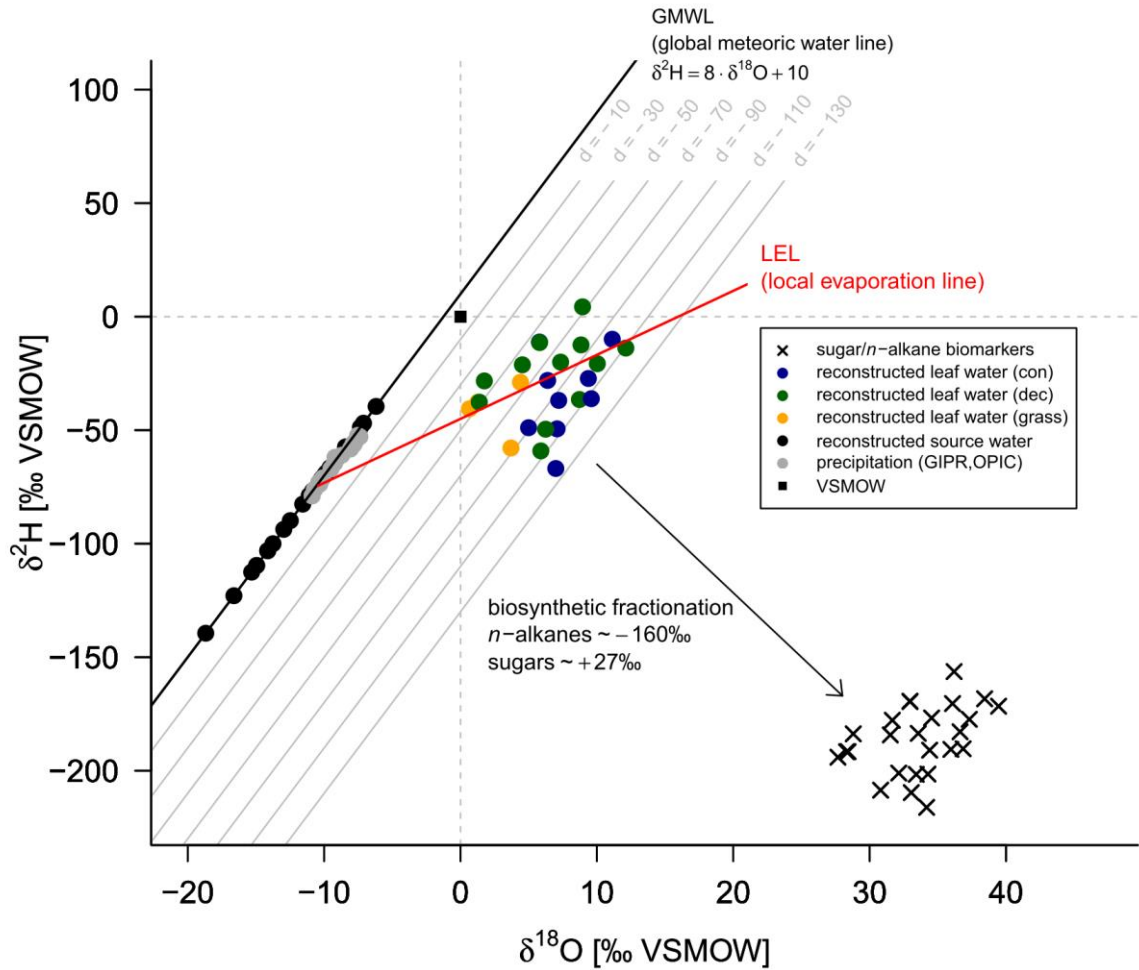
430 Based on the comparison of evapotranspirative enrichment between forest and grass sites, the
431 “signal damping” can be quantified to be ~ 31% for the hemicellulose sugars, and ~ 49% for
432 the *n*-alkanes. This is in agreement with other studies that reported a loss of 22% of the leaf

433 water enrichment for hemicellulose sugars (Helliker and Ehleringer, 2002) and 39 to 62% loss
 434 of the leaf water enrichment for *n*-alkanes (Gamarra et al., 2016).



435
 436 **Fig. 7.** Apparent fractionation (A) $\varepsilon_{n\text{-alkane/precipitation}}$ and (B) $\varepsilon_{\text{sugar/precipitation}}$. Biosynthetic
 437 fractionation factors according to section 2.4.2. Box plots show median (red line), interquartile
 438 range (IQR) with upper (75%) and lower (25%) quartiles, lowest whisker still within 1.5IQR
 439 of lower quartile, and highest whisker still within 1.5IQR of upper quartile, dots mark outliers.
 440 Abbreviations: con = coniferous forest sites (n=9); dec = deciduous forest sites (n=11 and 14
 441 for *n*-alkanes and sugars, respectively); grass = grassland sites (n=4 and 6 for *n*-alkanes and
 442 sugars, respectively). The figure conceptually illustrates the effect of biosynthetic fractionation
 443 and evapotranspirative enrichment as well as “signal damping”.

444
 445 **3.7 $\delta^2\text{H}_{\text{source-water}}$ and $\delta^{18}\text{O}_{\text{source-water}}$ reconstructions**
 446 The $\delta^2\text{H}$ versus $\delta^{18}\text{O}$ diagram shown in Fig. 8 graphically illustrates the reconstruction of $\delta^2\text{H}_{\text{leaf-water}}$
 447 and $\delta^{18}\text{O}_{\text{leaf-water}}$ (colored dots) from $\delta^2\text{H}_{n\text{-alkane}}$ and $\delta^{18}\text{O}_{\text{sugar}}$ (crosses), as well as the
 448 reconstruction of $\delta^2\text{H}_{\text{source-water}}$ and $\delta^{18}\text{O}_{\text{source-water}}$ (black dots). For reconstructing $\delta^2\text{H}_{\text{source-water}}$
 449 and $\delta^{18}\text{O}_{\text{source-water}}$, LELs with an average slope of 2.8 ± 0.1 (Eq. 10) can be generated through
 450 every leaf water point and the intercepts of these LELs with the GMWL.



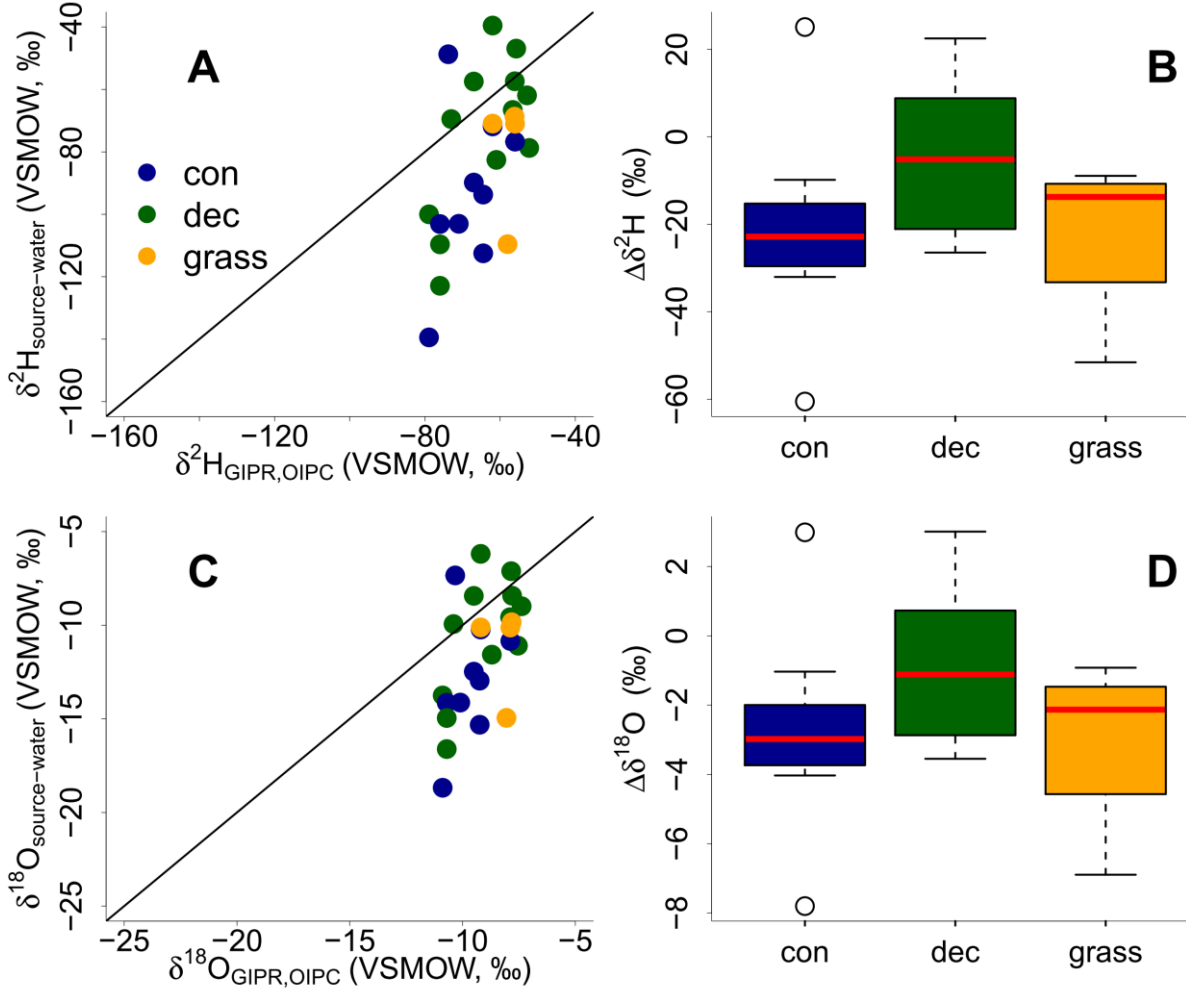
451
452 **Fig. 8.** $\delta^2\text{H}$ vs. $\delta^{18}\text{O}$ diagram illustrating the coupled $\delta^2\text{H}_{n\text{-alkane}}$ - $\delta^{18}\text{O}_{\text{sugar}}$ approach: measured
453 $\delta^2\text{H}_{n\text{-alkane}}$ and $\delta^{18}\text{O}_{\text{sugar}}$ values, reconstructed $\delta^2\text{H}_{\text{leaf-water}}$ and $\delta^{18}\text{O}_{\text{leaf-water}}$ (according Eqs. 8 and
454 9) and reconstructed $\delta^2\text{H}_{\text{source-water}}$ and $\delta^{18}\text{O}_{\text{source-water}}$ in comparison to GIPR and OIPC-based
455 $\delta^2\text{H}_{\text{precipitation}}$ and $\delta^{18}\text{O}_{\text{precipitation}}$. Abbreviations: con = coniferous forest sites (n=9); dec =
456 deciduous forest sites (n=11); grass = grassland sites (n=4).

457
458 The reconstructed $\delta^2\text{H}_{\text{source-water}}$ and $\delta^{18}\text{O}_{\text{source-water}}$ results can be compared with the $\delta^2\text{H}_{\text{GIPR,OIPC}}$
459 and $\delta^{18}\text{O}_{\text{GIPR,OIPC}}$ data (Fig. 9). This comparison reveals that the coupled $\delta^2\text{H}_{n\text{-alkane}}$ - $\delta^{18}\text{O}_{\text{sugar}}$
460 approach yields more accurate $\delta^2\text{H}_{\text{source-water}}$ and $\delta^{18}\text{O}_{\text{source-water}}$ compared to single $\delta^2\text{H}_{n\text{-alkane}}$
461 approaches. However, the range of the reconstructed $\delta^2\text{H}_{\text{source-water}}$ and $\delta^{18}\text{O}_{\text{source-water}}$ values is
462 clearly larger than in $\delta^2\text{H}_{\text{GIPR,OIPC}}$ and $\delta^{18}\text{O}_{\text{GIPR,OIPC}}$ values. $\delta^2\text{H}$ is systematically underestimated
463 by $\sim 21\text{‰} \pm 22$ (Fig. 9B) and $\delta^{18}\text{O}$ by $\sim 2.9\text{‰} \pm 2.8$ (Fig. 9D). The type of vegetation seems to
464 be not particularly relevant (p-value = 0.18 for $\Delta\delta^2\text{H}$ and p-value = 0.34 for $\Delta\delta^{18}\text{O}$).
465 Nevertheless, the systematic offsets tend to be lowest for the deciduous sites ($\Delta\delta^2\text{H}$ and $\Delta\delta^{18}\text{O}$ is
466 closer to zero with $\sim -5\text{‰} \pm 15$ and $\sim -1.1\text{‰} \pm 2.1$), followed by grass sites ($\sim -14\text{‰} \pm 20$ and \sim
467 $2.1\text{‰} \pm 2.6$). In comparison, the coniferous sites show the largest offsets ($\sim -23\text{‰} \pm 26$ for $\Delta\delta^2\text{H}$
468 $\sim -3.0\text{‰} \pm 3.3$ for $\Delta\delta^{18}\text{O}$). Differences are, however, not statistically significant. The systematic
469 offset and the large variability might have more specific reasons, and we suggest that this is
470 related to the type of vegetation. Deciduous trees produce lots of leaf waxes and sugars (e.g.
471 Prietzel et al., 2013; Zech et al., 2012a), and all biomarkers reflect and record the

472 evapotranspirative enrichment of the leaf water (e.g. Kahmen et al., 2013; Tuthorn et al., 2014).
473 However, coniferous trees produce quite low amounts of *n*-alkanes (Diefendorf and Freimuth,
474 2016; Zech et al., 2012a), while sugar concentrations are as high as in other vascular plants (e.g.
475 Hepp et al., 2016; Prietzel et al., 2013). For the coniferous soil samples this means that the *n*-
476 alkanes stem most likely from the understory whereas the sugars originate from grasses and
477 coniferous needles. When the understory is dominated by grass species then the *n*-alkane
478 biomarkers do not record the full leaf water enrichment signal, whereas the sugars from the
479 needles do. The reconstructed leaf water for the coniferous sites is therefore too negative
480 concerning $\delta^2\text{H}$, and reconstructed $\delta^2\text{H}_{\text{source-water}}$ and $\delta^{18}\text{O}_{\text{source-water}}$ values thus also become too
481 negative (Fig. 8). Concerning the grass sites the following explanation can be found. Correcting
482 for “signal damping” makes the reconstructed leaf water points more positive and shifts them
483 in Fig. 8 up and right. As the “signal damping” is stronger for $\delta^2\text{H}$ than for $\delta^{18}\text{O}$ the corrected
484 leaf water points would now above the uncorrected ones. The corrected leaf water points leads
485 to more positive reconstructed $\delta^2\text{H}_{\text{source-water}}$ and $\delta^{18}\text{O}_{\text{source-water}}$ values for the grass sites.
486 However, Gao et al. (2014) and Liu et al. (2016) showed that the ε_{bio} of monocotyledon plants
487 could larger than those of dicotyledonous once. This would therefore course a more negative
488 apparent fractionation factor for grasses compared to trees. We observe that the apparent
489 fractionation is indeed more negative for the grass sites compared to the forest sites. The effects
490 of “signal damping” vs. variable ε_{bio} along with vegetation types are indistinguishable here. As
491 an outlook for a future study, we therefore strongly recommend a comparison between the here
492 measured $\delta^2\text{H}_{n\text{-alkane}}$ values with modelled once using a new available model approach from
493 Konecky et al. (2019), which could provide insights if such vegetation effects on ε_{bio} of ^2H in
494 *n*-alkanes are describable.

495

496 Vegetation type specific rooting depths could partly cause the overall high variability in
497 reconstructed $\delta^2\text{H}_{\text{source-water}}$ and $\delta^{18}\text{O}_{\text{source-water}}$. Deep rooting species most likely use the water
498 from deeper soil horizons and/or shallow ground water, which is equal to the (weighted) mean
499 annual precipitation (e.g. Herrmann et al., 1987). Shallow rooting plants take up water from
500 upper soil horizons, which is influenced by seasonal variations in $\delta^2\text{H}_{\text{precipitation}}$ and $\delta^{18}\text{O}_{\text{precipitation}}$
501 and by soil water enrichment (Dubbert et al., 2013). Thus, the overall assumption that the source
502 water of the plants reflects the local (weighted) mean precipitation might be not fully valid for
503 all sites. Moreover, a partly contribution of root-derived rather than leaf-derived sugar
504 biomarkers in our topsoil samples is very likely. This does, by contrast, not apply for *n*-alkanes,
505 which are hardly produced in roots (Zech et al., 2012b and the discussion therein).



506
507 **Fig. 9.** Correlation of reconstructed $\delta^2\text{H}_{\text{source-water}}$ and $\delta^{18}\text{O}_{\text{source-water}}$ vs. precipitation $\delta^2\text{H}_{\text{GIPR,OIPC}}$
508 and $\delta^{18}\text{O}_{\text{GIPR,OIPC}}$ (A and C). Black lines indicate 1:1 relationship. Differences between
509 reconstructed source water and precipitation ($\Delta\delta^2\text{H}, \Delta\delta^{18}\text{O} = \delta^2\text{H}_{\text{source-water}}, \delta^{18}\text{O}_{\text{source-water}} -$
510 $\delta^2\text{H}_{\text{GIPR,OIPC}}, \delta^{18}\text{O}_{\text{GIPR,OIPC}})$ for the three different vegetation types (B and D). Box plots show
511 median (red line), interquartile range (IQR) with upper (75%) and lower (25%) quartiles, lowest
512 whisker still within 1.5IQR of lower quartile, and highest whisker still within 1.5IQR of upper
513 quartile. Abbreviations: con = coniferous forest sites (n=9); dec = deciduous forest sites (n=11);
514 grass = grassland sites (n=4).

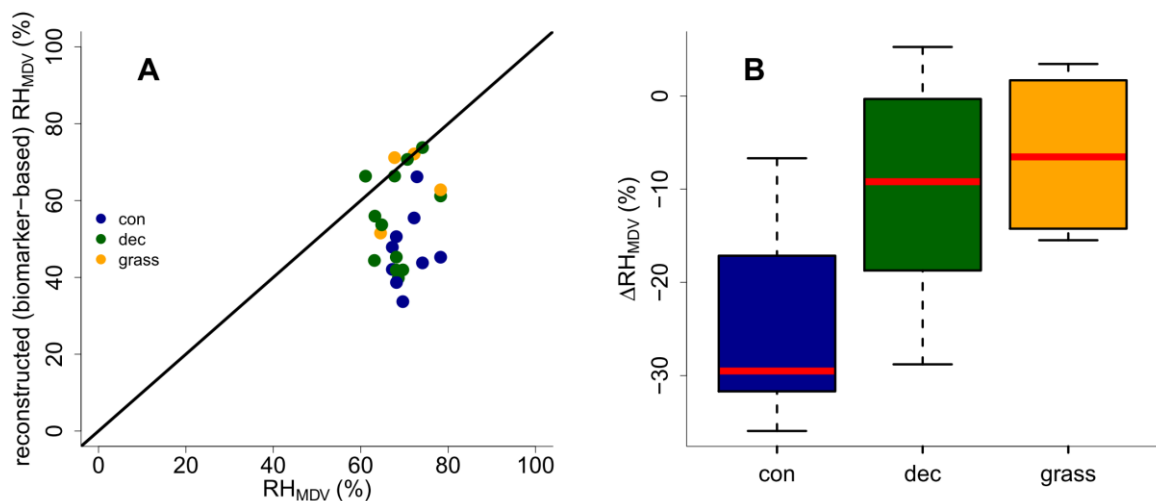
515 Moreover, the high variability within the vegetation types could be caused by variability in ε_{bio}
516 of ^2H in n -alkanes, as well as ^{18}O in sugars. There is an ongoing discussion about the correct
517 ε_{bio} for ^{18}O in hemicellulose sugars (Sternberg, 2014 vs. Zech et al., 2014), and ε_{bio} is probably
518 not constant over all vegetation types. This translates into errors concerning leaf water
519 reconstruction and thus for reconstructing $\delta^2\text{H}_{\text{source-water}}$ and $\delta^{18}\text{O}_{\text{source-water}}$ values (Eq. 9 and Fig.
520 8). Likewise, the ε_{bio} values reported in the literature for ^2H of n -alkanes can be off from -160‰
521 by tens of permille (Feakins and Sessions, 2010; Tipple et al., 2015; Feakins et al., 2016;
522 Freimuth et al., 2017). The degree to which hydrogen originates from NADPH rather than leaf
523 water is important, because NADPH is more negative (Schmidt et al., 2003). The wide range
524 in biosynthetic ^2H fractionation factors, which can be even larger, is therefore also related to
525 the carbon and energy metabolism state of plants (Cormier et al., 2018).

526 **3.8 RH reconstruction**

527 Reconstructed RH_{MDV} ranges from 34 to 74%, while RH_{MDV} from climate station data range
 528 from 61 to 78% (Fig. 10A). Biomarker-based values thus systematically underestimate the
 529 station data ($\Delta\text{RH}_{\text{MDV}} = -17\% \pm 12$). Yet the offsets are much less for deciduous tree and grass
 530 sites ($\Delta\text{RH}_{\text{MDV}} = -10\% \pm 12$ and $-7\% \pm 9$, respectively; Fig. 10B). The offsets for the coniferous
 531 sites are $-30\% \pm 11$, and significantly larger than for the deciduous and grass sites (p-values <
 532 0.05).

533 Too low reconstructed RH_{MDV} values for the coniferous sites make sense in view of the
 534 previously discussed option that soils contain *n*-alkanes from the understory (which is
 535 dominated by grass species), while sugars stem from needles and grasses. As explained earlier
 536 already, the “signal damping” leads to too negative reconstructed $\delta^2\text{H}_{\text{leaf-water}}$ (whereas $\delta^{18}\text{O}$ is
 537 affected less by the “signal damping”), and too negative $\delta^2\text{H}_{\text{leaf-water}}$ translates into
 538 overestimated d-excess and underestimated RH values. In Fig. 8, a correction for this require
 539 moving the coniferous leaf water data points upwards towards more positive $\delta^2\text{H}$ values, thus
 540 the distance between the leaf water and the source water is reduced. It should be noted that also
 541 here variable ε_{bio} along with vegetation types could not be distinguished from “signal damping”
 542 effects.

543 The underestimation of RH for the deciduous and grass sites could be partly associated with the
 544 use of the GMWL as baseline for the coupled $\delta^2\text{H}_{n\text{-alkane}}-\delta^{18}\text{O}_{\text{sugar}}$ approach. The deuterium-
 545 excess of the LMWLs is generally lower than the $+10\text{\textperthousand}$ of the GMWL, while the slopes of the
 546 LMWLs are well comparable to the GMWL (Stumpp et al., 2014). In addition, if soil water
 547 evaporation occurred before water uptake by the plants, this would lead to an underestimation
 548 of biomarker-based RH_{MDV} values. It can be furthermore assumed that plant metabolism is
 549 highest during times with direct sunshine and high irradiation, i.e. during noon at sunny days.
 550 The relevant RH could therefore be lower than the climate station-derived RH_{MDV}. Indeed,
 551 already climate station RH_{MDV} is considerable lower than RH_{MA} and RH_{MV} (Tab. S1).



552 **Fig. 10.** (A) Comparison of reconstructed (biomarker-based) RH_{MDV} values and climate station
 553 RH_{MDV} data. The black line indicates the 1:1 relationship. (B) Differences between
 554 reconstructed and climate station RH_{MDV} values ($\Delta\text{RH}_{\text{MDV}} = \text{reconstructed} - \text{climate station}$
 555 RH_{MDV}) for the three different vegetation types along the transect. Abbreviations: con =
 556 coniferous forest sites (n=9); dec = deciduous forest sites (n=11); grass = grassland sites (n=4).

558 The uncertainty of reconstructed RH_{MDV} values are large for all three investigated vegetation
559 types, and again these uncertainties are probably also related to ε_{bio} , which is most likely not
560 constant as assumed for our calculations. Moreover, microclimate variability is underestimated
561 in our approach. As mentioned in sections 2.4.2 and 3.7, in the coupled approach not only the
562 source water of the plants is equated with (weighted) mean annual precipitation, but also an
563 isotopic equilibrium between the source water and the (local) atmospheric water vapour is
564 assumed. However, in areas with distinct seasonality this might be not fully valid. To account
565 for this lack of equilibrium between precipitation and local atmospheric water vapour, apparent
566 ε values can be calculated with data from Jacob and Sonntag, (1991). As shown by Hepp et al.
567 (2018) those values can be used to achieve alternative RH reconstructions based on the coupled
568 $\delta^2\text{H}_{n\text{-alkane}}-\delta^{18}\text{O}_{\text{sugar}}$ approach. Such calculated RH_{MDV} values are on average 1.5% more
569 negative than the original values. However, this difference in RH is far below the analytical
570 uncertainties of the compound-specific biomarker isotope analysis.

571 Finally, the integration time of the investigated topsoils has to be discussed. Unfortunately, no
572 ^{14}C dates are available for the soil samples. However, most likely the organic matter has been
573 built up over a longer timescale than the available climate data, which is used for comparison.
574 In combination with vegetation changes/management changes throughout that period, this
575 could surely lead to a less tight relationship of the reconstructions compared to the climate
576 station data. Root input of arabinose and xylose seems to be of minor relevance in our topsoil
577 samples. Otherwise, the reconstructed $\delta^{18}\text{O}_{\text{sugar}}$ values would be too negative resulting in
578 RH_{MDV} overestimations, which is not observed.

579

580 4 Conclusions

581 We were able to show that

- 582 (i) the vegetation type does not significantly influence the brGDGT concentrations and
583 proxies, yet the coniferous sites tend to have higher brGDGT concentrations, BIT
584 indices and CBT-MBT' ratios, while grass sites tend to be lowest.
- 585 (ii) CBT faithfully records soil pH with a median ΔpH of 0.6 ± 0.6 , The CBT
586 overestimates the real pH particularly at the forest sites.
- 587 (iii) CBT-MBT'-derived T_{MA} reflect the climate station-derived T_{MA} values with a
588 median ΔT_{MA} of $0.5^{\circ}\text{C} \pm 2.4$, but again slightly too high reconstruction for the forest
589 sites were observed.
- 590 (iv) differences in the apparent fractionation between the investigated vegetation types
591 could caused by “signal damping” or variable ε_{bio} along with vegetation types, which
592 are indistinguishable here.
- 593 (v) the reconstructed $\delta^2\text{H}_{\text{source-water}}$ and $\delta^{18}\text{O}_{\text{source-water}}$ reflects the $\delta^2\text{H}_{\text{GIPR,OIPC}}$ and
594 $\delta^{18}\text{O}_{\text{GIPR,OIPC}}$ with a systematic offset for $\delta^2\text{H}$ of $\sim -21\% \pm 22$ and for $\delta^{18}\text{O}$ of $\sim -2.9\% \pm 2.8$
595 (based on overall medians of $\Delta\delta^2\text{H}$, $\delta^{18}\text{O}$). This is caused by too negative
596 reconstructions for coniferous and grass sites. For coniferous sites, this can be
597 explained with *n*-alkanes originating from understory grasses. As for the grass sites,
598 the “signal damping” or variable ε_{bio} along with vegetation types more effect $\delta^2\text{H}$

599 than $\delta^{18}\text{O}$. This leads to too negative reconstructed $\delta^2\text{H}_{\text{leaf-water}}$ values and thus to too
600 negative $\delta^2\text{H}_{\text{source-water}}$ and $\delta^{18}\text{O}_{\text{source-water}}$ reconstructions.

601 (vi) reconstructed (biomarker-based) RH_{MDV} values tend to underestimate climate
602 station-derived RH_{MDV} values ($\Delta\text{RH}_{\text{MDV}} = \sim -17\% \pm 12$). For coniferous sites the
603 underestimations are strongest, which can be explained with understory grasses
604 being the main source of *n*-alkanes for the investigated soils under coniferous
605 forests.

606 Overall, our study highlights the great potential of GDGTs and the coupled $\delta^2\text{H}_{n\text{-alkane}}-\delta^{18}\text{O}_{\text{sugar}}$
607 approach for more quantitative paleoclimate reconstructions. Taking into account effects of
608 different vegetation types improves correlations and reconstructions. This holds particularly
609 true for the coupled $\delta^2\text{H}_{n\text{-alkane}}-\delta^{18}\text{O}_{\text{sugar}}$ approach, which is affected by “signal damping” of the
610 grass vegetation or variable ε_{bio} along with vegetation types. Assuming constant biosynthetic
611 fractionation is likely a considerable source of uncertainty and should be in focus in future field
612 and/or modelling studies. Climate chamber experiments would be very useful to further
613 evaluate and refine the coupled $\delta^2\text{H}_{n\text{-alkane}}-\delta^{18}\text{O}_{\text{sugar}}$ approach, because uncertainties related to
614 microclimate variability can be reduced. Field experiments like ours suffer from the fact that
615 biomarker pools in the sampled topsoils may have been affected by past vegetation and climate
616 changes.

617

618 Acknowledgements

619 We thank L. Wüthrich, H. Veit, T. Sprafke, A. Groos (all University of Bern), A. Kühnel
620 (Technical University of Munich) for constructive discussions and statistical advices, and M.
621 Schaarschmidt (University of Bayreuth), C. Heinrich and M. Benesch (Martin-Luther-
622 University Halle-Wittenberg) for laboratory assistance during $\delta^{18}\text{O}_{\text{sugar}}$ analysis and pH
623 measurements, respectively. The Swiss National Science Foundation (PP00P2 150590) funded
624 this research. J. Hepp greatly acknowledges the support by the German Federal Environmental
625 Foundation (DBU) in form of his PhD-fellowship.

626

627 References

628 Allison, G. B., Gat, J. R. and Leaney, F. W. J.: The relationship between deuterium and oxygen-
629 18 delta values in leaf water, *Chemical Geology*, 58, 145–156, 1985.

630 Amelung, W., Cheshire, M. V. and Guggenberger, G.: Determination of neutral and acidic
631 sugars in soil by capillary gas-liquid chromatography after trifluoroacetic acid hydrolysis,
632 *Soil Biology and Biochemistry*, 28(12), 1631–1639, 1996.

633 Anderson, V. J., Shanahan, T. M., Saylor, J. E., Horton, B. K. and Mora, A. R.: Sources of local
634 and regional variability in the MBT'/CBT paleotemperature proxy: Insights from a
635 modern elevation transect across the Eastern Cordillera of Colombia, *Organic
636 Geochemistry*, 69, 42–51, doi:10.1016/j.orggeochem.2014.01.022, 2014.

637 Awe, G. O., Reichert, J. M. and Wendroth, O. O.: Temporal variability and covariance
638 structures of soil temperature in a sugarcane field under different management practices
639 in southern Brazil, *Soil and Tillage Research*, 150, 93–106,

640 doi:10.1016/j.still.2015.01.013, 2015.

641 Bariac, T., Gonzalez-Dunia, J., Katerji, N., Béthenod, O., Bertolini, J. M. and Mariotti, A.:
642 Spatial variation of the isotopic composition of water (^{18}O , ^2H) in the soil-plant-
643 atmosphere system, 2. Assessment under field conditions, *Chemical Geology*, 115, 317–
644 333, 1994.

645 Bowen, G. J.: The Online Isotopes in Precipitation Calculator, version 3.1., 2018.

646 Bowen, G. J. and Revenaugh, J.: Interpolating the isotopic composition of modern meteoric
647 precipitation, *Water Resources Research*, 39(10), 1–13, doi:10.1029/2003WR002086,
648 2003.

649 Brincat, D., Yamada, K., Ishiwatari, R., Uemura, H. and Naraoka, H.: Molecular-isotopic
650 stratigraphy of long-chain *n*-alkanes in Lake Baikal Holocene and glacial age sediments,
651 *Organic Geochemistry*, 31(4), 287–294, doi:10.1016/S0146-6380(99)00164-3, 2000.

652 Cappelen, J.: Danish Climatological Normals 1971-2000 - for selected stations., 2002.

653 Cernusak, L. A., Wong, S. C. and Farquhar, G. D.: Oxygen isotope composition of phloem sap
654 in relation to leaf water in *Ricinus communis*, *Functional Plant Biology*, 30(10), 1059–
655 1070, 2003.

656 Cernusak, L. A., Barbour, M. M., Arndt, S. K., Cheesman, A. W., English, N. B., Feild, T. S.,
657 Helliker, B. R., Holloway-Phillips, M. M., Holtum, J. A. M., Kahmen, A., Mcinerney, F.
658 A., Munksgaard, N. C., Simonin, K. A., Song, X., Stuart-Williams, H., West, J. B. and
659 Farquhar, G. D.: Stable isotopes in leaf water of terrestrial plants, *Plant Cell and
660 Environment*, 39(5), 1087–1102, doi:10.1111/pce.12703, 2016.

661 Christoph, H., Eglinton, T. I., Zech, W., Sosin, P. and Zech, R.: A 250 ka leaf-wax δD record
662 from a loess section in Darai Kalon , Southern Tajikistan, *Quaternary Science Reviews*,
663 208, 118–128, doi:10.1016/j.quascirev.2019.01.019, 2019.

664 Coffinet, S., Huguet, A., Anquetil, C., Derenne, S., Pedentchouk, N., Bergonzini, L.,
665 Omumbo, C., Williamson, D., Jones, M., Majule, A. and Wagner, T.: Evaluation of
666 branched GDGTs and leaf wax *n*-alkane $\delta^2\text{H}$ as (paleo) environmental proxies in East
667 Africa, *Geochimica et Cosmochimica Acta*, 198, 182–193,
668 doi:10.1016/j.gca.2016.11.020, 2017.

669 Cormier, M.-A., Werner, R. A., Sauer, P. E., Gröcke, D. R., M.C., L., Wieloch, T., Schleucher,
670 J. and Kahmen, A.: ^2H fractiontions during the biosynthesis of carbohydrates and lipids
671 imprint a metabolic signal on the $\delta^2\text{H}$ values of plant organic compounds, *New
672 Phytologist*, 218(2), 479–491, doi:10.1111/nph.15016, 2018.

673 Craig, H.: Isotopic Variations in Meteoric Waters, *Science*, 133, 1702–1703, 1961.

674 Dang, X., Yang, H., Naafs, B. D. A., Pancost, R. D. and Xie, S.: Evidence of moisture control
675 on the methylation of branched glycerol dialkyl glycerol tetraethers in semi-arid and arid
676 soils, *Geochimica et Cosmochimica Acta*, 189, 24–36, doi:10.1016/j.gca.2016.06.004,
677 2016.

678 Dansgaard, W.: Stable isotopes in precipitation, *Tellus*, 16(4), 436–468, doi:10.1111/j.2153-
679 3490.1964.tb00181.x, 1964.

680 Dawson, T. E., Mambelli, S., Plamboeck, A. H., Templer, P. H. and Tu, K. P.: Stable Isotopes
681 in Plant Ecology, *Annual Review of Ecology and Systematics*, 33(1), 507–559,
682 doi:10.1146/annurev.ecolsys.33.020602.095451, 2002.

683 Diefendorf, A. F. and Freimuth, E. J.: Extracting the most from terrestrial plant-derived *n*-alkyl
684 lipids and their carbon isotopes from the sedimentary record: A review, *Organic*
685 *Geochemistry*, 103(January), 1–21, doi:10.1016/j.orggeochem.2016.10.016, 2016.

686 Dirghangi, S. S., Pagani, M., Hren, M. T. and Tipple, B. J.: Distribution of glycerol dialkyl
687 glycerol tetraethers in soils from two environmental transects in the USA, *Organic*
688 *Geochemistry*, 59, 49–60, doi:10.1016/j.orggeochem.2013.03.009, 2013.

689 Dubbert, M., Cuntz, M., Piayda, A., Maguás, C. and Werner, C.: Partitioning evapotranspiration
690 - Testing the Craig and Gordon model with field measurements of oxygen isotope ratios
691 of evaporative fluxes, *Journal of Hydrology*, 496, 142–153,
692 doi:10.1016/j.jhydrol.2013.05.033, 2013.

693 DWD Climate Data Center: Historical annual precipitation observations for Germany. [online]
694 Available from: [ftp://ftp-](ftp://ftp-cdc.dwd.de/pub/CDC/observations_germany/climate/hourly/precipitation/historical/)
695 (Accessed 20 September 2018a), 2018.

696

697 DWD Climate Data Center: Historical hourly station observations of 2m air temperature and
698 humidity for Germany. [online] Available from: [ftp://ftp-](ftp://ftp-cdc.dwd.de/pub/CDC/observations_germany/climate/hourly/air_temperature/historical/)
699 (Accessed 19 September 2018b), 2018.

700

701 Eglinton, T. I. and Eglinton, G.: Molecular proxies for paleoclimatology, *Earth and Planetary*
702 *Science Letters*, 275(1), 1–16, 2008.

703 Feakins, S. J. and Sessions, A. L.: Controls on the D/H ratios of plant leaf waxes in an arid
704 ecosystem, *Geochimica et Cosmochimica Acta*, 74(7), 2128–2141,
705 doi:<http://dx.doi.org/10.1016/j.gca.2010.01.016>, 2010.

706 Feakins, S. J., Bentley, L. P., Salinas, N., Shenkin, A., Blonder, B., Goldsmith, G. R., Ponton,
707 C., Arvin, L. J., Wu, M. S., Peters, T., West, A. J., Martin, R. E., Enquist, B. J., Asner, G.
708 P. and Malhi, Y.: Plant leaf wax biomarkers capture gradients in hydrogen isotopes of
709 precipitation from the Andes and Amazon, *Geochimica et Cosmochimica Acta*, 182, 155–
710 172, doi:10.1016/j.gca.2016.03.018, 2016.

711 Freimuth, E. J., Diefendorf, A. F. and Lowell, T. V.: Hydrogen isotopes of *n*-alkanes and *n*-
712 alkanoic acids as tracers of precipitation in a temperate forest and implications for
713 paleorecords, *Geochimica et Cosmochimica Acta*, 206, 166–183,
714 doi:10.1016/j.gca.2017.02.027, 2017.

715 Frich, P., Rosenørn, S., Madsen, H. and Jensen, J. J.: Observed Precipitation in Denmark, 1961–
716 90., 1997.

717 Gamarra, B., Sachse, D. and Kahmen, A.: Effects of leaf water evaporative ^2H -enrichment and
718 biosynthetic fractionation on leaf wax *n*-alkane $\delta^2\text{H}$ values in C3 and C4 grasses, *Plant,*
719 *Cell and Environment Environment*, 39, 2390–2403, doi:10.1111/pce.12789, 2016.

720 Gat, J. R.: Comments on the Stable Isotope Method in Regional Groundwater Investigations,
721 *Water Resources Research*, 7(4), 980–993, doi:10.1029/WR007i004p00980, 1971.

722 van Geldern, R., Baier, A., Subert, H. L., Kowol, S., Balk, L. and Barth, J. A. C.: (Table S1)
723 Stable isotope composition of precipitation sampled at Erlangen, Germany between 2010
724 and 2013 for station GeoZentrum located at Erlangen city center, in In supplement to: van
725 Geldern, R et al. (2014): Pleistocene paleo-groundwater as a pristine fresh water resource
726 in southern Germany – evidence from stable and radiogenic isotopes. *Science of the Total*

727 Environment, 496, 107-115, <https://doi.org/10.1016/j.pangaea>, 2014.

728 Guggenberger, G., Christensen, B. T. and Zech, W.: Land-use effects on the composition of
729 organic matter in particle-size separates of soil: I. Lignin and carbohydrate signature,
730 European Journal of Soil Science, 45(December), 449–458, 1994.

731 Helliker, B. R. and Ehleringer, J. R.: Grass blades as tree rings: environmentally induced
732 changes in the oxygen isotope ratio of cellulose along the length of grass blades, New
733 Phytologist, 155, 417–424, 2002.

734 Hepp, J., Rabus, M., Anhäuser, T., Bromm, T., Laforsch, C., Sirocko, F., Glaser, B. and Zech,
735 M.: A sugar biomarker proxy for assessing terrestrial versus aquatic sedimentary input,
736 Organic Geochemistry, 98, 98–104, doi:10.1016/j.orggeochem.2016.05.012, 2016.

737 Hepp, J., Wüthrich, L., Bromm, T., Bliedtner, M., Schäfer, I. K., Glaser, B., Rozanski, K.,
738 Sirocko, F., Zech, R. and Zech, M.: How dry was the Younger Dryas? Evidence from a
739 coupled $\delta^2\text{H}$ - $\delta^{18}\text{O}$ biomarker paleohygrometer, applied to the Lake Gemündener Maar
740 sediments, Western Eifel, Germany, Climate of the Past Discussions, (September), 1–44,
741 doi:10.5194/cp-2018-114, 2018.

742 Herrmann, A., Maloszewski, P. and Stichler, W.: Changes of ^{18}O contents of precipitation water
743 during seepage in the unsaturated zone, in Proceedings of International Symposium on
744 Groundwater Monitoring and Management, 23 - 28 March, p. 22, Institut of Water
745 Management Berlin (GDR) with support of UNESCO, Dresden., 1987.

746 Hopmans, E. C., Weijers, J. W. H., Schefuß, E., Herfort, L., Sinninghe Damsté, J. S. and
747 Schouten, S.: A novel proxy for terrestrial organic matter in sediments based on branched
748 and isoprenoid tetraether lipids, Earth and Planetary Science Letters, 224(1–2), 107–116,
749 doi:10.1016/j.epsl.2004.05.012, 2004.

750 Horita, J. and Wesolowski, D. J.: Liquid-vapor fractionation of oxygen and hydrogen isotopes
751 of water from the freezing to the critical temperature, Geochimica et Cosmochimica Acta,
752 58(16), 3425–3437, doi:[http://dx.doi.org/10.1016/0016-7037\(94\)90096-5](http://dx.doi.org/10.1016/0016-7037(94)90096-5), 1994.

753 Hothorn, T., Bühlmann, P., Dudoit, S., Molinaro, A. and Van Der Laan, M. J.: Survival
754 ensembles, Biostatistics, 7(3), 355–373, doi:10.1093/biostatistics/kxj011, 2006.

755 Hou, J., D'Andrea, W. J. and Huang, Y.: Can sedimentary leaf waxes record D/H ratios of
756 continental precipitation? Field, model, and experimental assessments, Geochimica et
757 Cosmochimica Acta, 72, 3503–3517, doi:10.1016/j.gca.2008.04.030, 2008.

758 Huguet, A., Fosse, C., Metzger, P., Fritsch, E. and Derenne, S.: Occurrence and distribution of
759 extractable glycerol dialkyl glycerol tetraethers in podzols, Organic Geochemistry, 41(3),
760 291–301, doi:10.1016/j.orggeochem.2009.10.007, 2010a.

761 Huguet, A., Fosse, C., Laggoun-Défarge, F., Toussaint, M. L. and Derenne, S.: Occurrence and
762 distribution of glycerol dialkyl glycerol tetraethers in a French peat bog, Organic
763 Geochemistry, 41(6), 559–572, doi:10.1016/j.orggeochem.2010.02.015, 2010b.

764 IAEA/WMO: Global Network of Isotopes in Precipitation. The GNIP Database., 2015.

765 IAEA/WMO: Global Network of Isotopes in Precipitation. The GNIP Database., 2018.

766 Jacob, H. and Sonntag, C.: An 8-year record of the seasonal- variation of ^2H and ^{18}O in
767 atmospheric water vapor and precipitation at Heidelberg, Tellus, 43B(3), 291–300, 1991.

768 De Jonge, C., Hopmans, E. C., Zell, C. I., Kim, J. H., Schouten, S. and Sinninghe Damsté, J.

769 S.: Occurrence and abundance of 6-methyl branched glycerol dialkyl glycerol tetraethers
770 in soils: Implications for palaeoclimate reconstruction, *Geochimica et Cosmochimica
771 Acta*, 141, 97–112, doi:10.1016/j.gca.2016.03.038, 2014.

772 Kahmen, A., Schefuß, E. and Sachse, D.: Leaf water deuterium enrichment shapes leaf wax *n*-
773 alkane δ D values of angiosperm plants I: Experimental evidence and mechanistic
774 insights, *Geochimica et Cosmochimica Acta*, 111, 39–49, doi:10.1016/j.gca.2012.09.004,
775 2013.

776 Knapp, D. R.: *Handbook of Analytical Derivatization Reactions*, John Wiley & Sons, New
777 York, Chichester, Brisbane, Toronto, Singapore., 1979.

778 Konecky, B., Dee, S. G. and Noone, D. C.: WaxPSM: A Forward Model of Leaf Wax Hydrogen
779 Isotope Ratios to Bridge Proxy and Model Estimates of Past Climate, *Journal of
780 Geophysical Research: Biogeosciences*, 124, 2107–2125, doi:10.1029/2018JG004708,
781 2019.

782 Laursen, E. V., Thomsen, R. S. and Cappelen, J.: Observed Air Temperature, Humidity,
783 Pressure, Cloud Cover and Weather in Denmark - with Climatological Standard Normals,
784 1961-90., 1999.

785 Levene, H.: Robust Tests for Equality of Variances, in *Contributions to Probability and
786 Statistics: Essays in Honor of Harold Hotelling*, vol. 69, edited by I. Olkin, pp. 78–92,
787 Standford University Press, Palo Alto, California., 1960.

788 Liu, W. and Yang, H.: Multiple controls for the variability of hydrogen isotopic compositions
789 in higher plant *n*-alkanes from modern ecosystems, *Global Change Biology*, 14(9), 2166–
790 2177, doi:10.1111/j.1365-2486.2008.01608.x, 2008.

791 Liu, Y., Wang, J., Liu, D., Li, Z., Zhang, G., Tao, Y., Xie, J., Pan, J. and Chen, F.: Straw
792 mulching reduces the harmful effects of extreme hydrological and temperature conditions
793 in citrus orchards, *PLoS ONE*, 9(1), 1–9, doi:10.1371/journal.pone.0087094, 2014.

794 McInerney, F. A., Helliker, B. R. and Freeman, K. H.: Hydrogen isotope ratios of leaf wax *n*-
795 alkanes in grasses are insensitive to transpiration, *Geochimica et Cosmochimica Acta*,
796 75(2), 541–554, doi:10.1016/j.gca.2010.10.022, 2011.

797 Merlivat, L.: Molecular diffusivities of $H_2^{16}O$, $HD^{16}O$, and $H_2^{18}O$ in gases, *The Journal of
798 Chemical Physics*, 69(6), 2864–2871, doi:<http://dx.doi.org/10.1063/1.436884>, 1978.

799 Mueller-Niggemann, C., Utami, S. R., Marxen, A., Mangelsdorf, K., Bauersachs, T. and
800 Schwark, L.: Distribution of tetraether lipids in agricultural soils - Differentiation
801 between paddy and upland management, *Biogeosciences*, 13(5), 1647–1666,
802 doi:10.5194/bg-13-1647-2016, 2016.

803 Oppermann, B. I., Michaelis, W., Blumenberg, M., Frerichs, J., Schulz, H. M., Schippers, A.,
804 Beaubien, S. E. and Krüger, M.: Soil microbial community changes as a result of long-
805 term exposure to a natural CO₂ vent, *Geochimica et Cosmochimica Acta*, 74(9), 2697–
806 2716, doi:10.1016/j.gca.2010.02.006, 2010.

807 Pedentchouk, N. and Zhou, Y.: Factors Controlling Carbon and Hydrogen Isotope Fractionation
808 During Biosynthesis of Lipids by Phototrophic Organisms, in *Hydrocarbons, Oils and
809 Lipids: Diversity, Origin, Chemistry and Fate. Handbook of Hydrocarbon and Lipid
810 Microbiology*, edited by H. Wilkes, pp. 1–24, Springer, Cham., 2018.

811 Peterse, F., van der Meer, J., Schouten, S., Weijers, J. W. H., Fierer, N., Jackson, R. B., Kim,

812 J. H. and Sinninghe Damsté, J. S.: Revised calibration of the MBT-CBT paleotemperature
813 proxy based on branched tetraether membrane lipids in surface soils, *Geochimica et*
814 *Cosmochimica Acta*, 96, 215–229, doi:10.1016/j.gca.2012.08.011, 2012.

815 Prietzel, J., Dechamps, N. and Spielvogel, S.: Analysis of non-cellulosic polysaccharides helps
816 to reveal the history of thick organic surface layers on calcareous Alpine soils, *Plant and*
817 *Soil*, 365(1–2), 93–114, doi:10.1007/s11104-012-1340-2, 2013.

818 R Core Team: R: A Language and Environment for Statistical Computing, [online] Available
819 from: <https://www.r-project.org/>, 2015.

820 Rach, O., Brauer, A., Wilkes, H. and Sachse, D.: Delayed hydrological response to Greenland
821 cooling at the onset of the Younger Dryas in western Europe, *Nature Geoscience*, 7(1),
822 109–112, doi:10.1038/ngeo2053, 2014.

823 Rao, Z., Zhu, Z., Jia, G., Henderson, A. C. G., Xue, Q. and Wang, S.: Compound specific δD
824 values of long chain *n*-alkanes derived from terrestrial higher plants are indicative of the
825 δD of meteoric waters: Evidence from surface soils in eastern China, *Organic*
826 *Geochemistry*, 40(8), 922–930, doi:<http://dx.doi.org/10.1016/j.orggeochem.2009.04.011>,
827 2009.

828 Romero-Viana, L., Kienel, U. and Sachse, D.: Lipid biomarker signatures in a hypersaline lake
829 on Isabel Island (Eastern Pacific) as a proxy for past rainfall anomaly (1942–2006AD),
830 *Palaeogeography, Palaeoclimatology, Palaeoecology*, 350–352, 49–61,
831 doi:10.1016/j.palaeo.2012.06.011, 2012.

832 Sachse, D., Radke, J. and Gleixner, G.: Hydrogen isotope ratios of recent lacustrine sedimentary
833 *n*-alkanes record modern climate variability, *Geochimica et Cosmochimica Acta*, 68(23),
834 4877–4889, doi:<http://dx.doi.org/10.1016/j.gca.2004.06.004>, 2004.

835 Sachse, D., Radke, J. and Gleixner, G.: δD values of individual *n*-alkanes from terrestrial plants
836 along a climatic gradient – Implications for the sedimentary biomarker record, *Organic*
837 *Geochemistry*, 37, 469–483, doi:10.1016/j.orggeochem.2005.12.003, 2006.

838 Sachse, D., Billault, I., Bowen, G. J., Chikaraishi, Y., Dawson, T. E., Feakins, S. J., Freeman,
839 K. H., Magill, C. R., McInerney, F. A., van der Meer, M. T. J., Polissar, P., Robins, R. J.,
840 Sachs, J. P., Schmidt, H.-L., Sessions, A. L., White, J. W. C. and West, J. B.: Molecular
841 Paleohydrology: Interpreting the Hydrogen-Isotopic Composition of Lipid Biomarkers
842 from Photosynthesizing Organisms, *Annual Reviews*, 40, 221–249,
843 doi:10.1146/annurev-earth-042711-105535, 2012.

844 Schäfer, I. K., Lanny, V., Franke, J., Eglinton, T. I., Zech, M., Vysloužilová, B. and Zech, R.:
845 Leaf waxes in litter and topsoils along a European transect, *SOIL*, 2, 551–564,
846 doi:10.5194/soil-2-551-2016, 2016.

847 Schlotter, D.: The spatio-temporal distribution of $\delta^{18}\text{O}$ and $\delta^2\text{H}$ of precipitation in Germany -
848 an evaluation of regionalization methods, Albert-Ludwigs-Universität Freiburg im
849 Breisgau. [online] Available from: http://www.hydrology.uni-freiburg.de/abschluss/Schlotter_D_2007_DA.pdf, 2007.

851 Schmidt, H.-L., Werner, R. A. and Roßmann, A.: ^{18}O Pattern and biosynthesis of natural plant
852 products, *Phytochemistry*, 58(1), 9–32, doi:[http://dx.doi.org/10.1016/S0031-9422\(01\)00017-6](http://dx.doi.org/10.1016/S0031-9422(01)00017-6), 2001.

854 Schmidt, H.-L., Werner, R. A. and Eisenreich, W.: Systematics of ^2H patterns in natural
855 compounds and its importance for the elucidation of biosynthetic pathways,

856 Phytochemistry Reviews, 2(1–2), 61–85, doi:10.1023/B:PHYT.0000004185.92648.ae,
857 2003.

858 Schouten, S., Hopmans, E. C. and Sinninghe Damsté, J. S.: The organic geochemistry of
859 glycerol dialkyl glycerol tetraether lipids: A review, *Organic Geochemistry*, 54, 19–61,
860 doi:10.1016/j.orggeochem.2012.09.006, 2013.

861 Schreuder, L. T., Beets, C. J., Prins, M. A., Hatté, C. and Peterse, F.: Late Pleistocene climate
862 evolution in Southeastern Europe recorded by soil bacterial membrane lipids in Serbian
863 loess, *Palaeogeography, Palaeoclimatology, Palaeoecology*, 449, 141–148,
864 doi:10.1016/j.palaeo.2016.02.013, 2016.

865 Sessions, A. L., Burgoyne, T. W., Schimmelmann, A. and Hayes, J. M.: Fractionation of
866 hydrogen isotopes in lipid biosynthesis, *Organic Geochemistry*, 30, 1193–1200, 1999.

867 Shapiro, S. S. and Wilk, M. B.: An Analysis of Variance Test for Normality, *Biometrika*,
868 52(3/4), 591–611, doi:/biomet/52.3-4.591, 1965.

869 Sternberg, L. S. L.: Comment on “Oxygen isotope ratios ($^{18}\text{O}/^{16}\text{O}$) of hemicellulose-derived
870 sugar biomarkers in plants, soils and sediments as paleoclimate proxy I: Insight from a
871 climate chamber experiment” by Zech et al. (2014), *Geochimica et Cosmochimica Acta*,
872 141, 677–679, doi:10.1016/j.gca.2014.04.051, 2014.

873 Strobl, C., Boulesteix, A. L., Zeileis, A. and Hothorn, T.: Bias in random forest variable
874 importance measures: Illustrations, sources and a solution, *BMC Bioinformatics*, 8,
875 doi:10.1186/1471-2105-8-25, 2007.

876 Strobl, C., Boulesteix, A. L., Kneib, T., Augustin, T. and Zeileis, A.: Conditional variable
877 importance for random forests, *BMC Bioinformatics*, 9, 1–11, doi:10.1186/1471-2105-9-
878 307, 2008.

879 Stumpp, C., Klaus, J. and Stichler, W.: Analysis of long-term stable isotopic composition in
880 German precipitation, *Journal of Hydrology*, 517, 351–361,
881 doi:10.1016/j.jhydrol.2014.05.034, 2014.

882 Sun, C. J., Zhang, C. L., Li, F. Y., Wang, H. Y. and Liu, W. G.: Distribution of branched
883 glycerol dialkyl glycerol tetraethers in soils on the Northeastern Qinghai-Tibetan Plateau
884 and possible production by nitrite-reducing bacteria, *Science China Earth Sciences*, 59(9),
885 1834–1846, doi:10.1007/s11430-015-0230-2, 2016.

886 Swedish Meteorological and Hydrological Institute: SMHI Open Data Meteorological
887 Observations., 2018.

888 Tippie, B. J., Berke, M. A., Hambach, B., Roden, J. S. and Ehleringer, J. R.: Predicting leaf
889 wax *n*-alkane $^{2}\text{H}/^{1}\text{H}$ ratios: Controlled water source and humidity experiments with
890 hydroponically grown trees confirm predictions of Craig-Gordon model, *Plant, Cell and
891 Environment*, 38(6), 1035–1047, doi:10.1111/pce.12457, 2015.

892 Tuthorn, M., Zech, M., Ruppenthal, M., Oelmann, Y., Kahmen, A., del Valle, H. F., Wilcke,
893 W. and Glaser, B.: Oxygen isotope ratios ($^{18}\text{O}/^{16}\text{O}$) of hemicellulose-derived sugar
894 biomarkers in plants, soils and sediments as paleoclimate proxy II: Insight from a climate
895 transect study, *Geochimica et Cosmochimica Acta*, 126, 624–634,
896 doi:<http://dx.doi.org/10.1016/j.gca.2013.11.002>, 2014.

897 Tuthorn, M., Zech, R., Ruppenthal, M., Oelmann, Y., Kahmen, A., del Valle, H. F., Eglinton,
898 T., Rozanski, K. and Zech, M.: Coupling $\delta^{2}\text{H}$ and $\delta^{18}\text{O}$ biomarker results yields

899 information on relative humidity and isotopic composition of precipitation - a climate
900 transect validation study, *Biogeosciences*, 12, 3913–3924, doi:10.5194/bg-12-3913-
901 2015, 2015.

902 Umweltbundesamt GmbH: Erhebung der Wassergüte in Österreich gemäß Hydrographiegesetz
903 i.d.F. des BGBI. Nr. 252/90 (gültig bis Dezember 2006) bzw.
904 Gewässerzustandsüberwachung in Österreich gemäß Wasserrechtsgesetz, BGBI. I Nr.
905 123/06, i.d.g.F.; BMLFUW, Sektion IV / Abteilung 3 N. [online] Available from:
906 <https://wasser.umweltbundesamt.at/h2odbfivestep/abfrageQdPublic.xhtml> (Accessed 20
907 September 2018), 2018.

908 Walker, C. D. and Brunel, J.-P.: Examining Evapotranspiration in a Semi-Arid Region using
909 Stable Isotopes of Hydrogen and Oxygen, *Journal of Hydrology*, 118, 55–75, 1990.

910 Wang, C., Hren, M. T., Hoke, G. D., Liu-Zeng, J. and Garzione, C. N.: Soil *n*-alkane δ D and
911 glycerol dialkyl glycerol tetraether (GDGT) distributions along an altitudinal transect
912 from southwest China: Evaluating organic molecular proxies for paleoclimate and
913 paleoelevation, *Organic Geochemistry*, 107, 21–32,
914 doi:10.1016/j.orggeochem.2017.01.006, 2017.

915 Wang, H., Liu, W., Zhang, C. L., Liu, Z. and He, Y.: Branched and isoprenoid tetraether (BIT)
916 index traces water content along two marsh-soil transects surrounding Lake Qinghai:
917 Implications for paleo-humidity variation, *Organic Geochemistry*, 59, 75–81,
918 doi:10.1016/j.orggeochem.2013.03.011, 2013.

919 Weijers, J. W. H., Schouten, S., Spaargaren, O. C. and Sinninghe Damsté, J. S.: Occurrence
920 and distribution of tetraether membrane lipids in soils: Implications for the use of the
921 TEX₈₆ proxy and the BIT index, *Organic Geochemistry*, 37(12), 1680–1693,
922 doi:10.1016/j.orggeochem.2006.07.018, 2006.

923 Weijers, J. W. H., Schouten, S., van den Donker, J. C., Hopmans, E. C. and Sinninghe Damsté,
924 J. S.: Environmental controls on bacterial tetraether membrane lipid distribution in soils,
925 *Geochimica et Cosmochimica Acta*, 71(3), 703–713, doi:10.1016/j.gca.2006.10.003,
926 2007.

927 Weijers, J. W. H., Wiesenberg, G. L. B., Bol, R., Hopmans, E. C. and Pancost, R. D.: Carbon
928 isotopic composition of branched tetraether membrane lipids in soils suggest a rapid
929 turnover and a heterotrophic life style of their source organism(s), *Biogeosciences*, 7(9),
930 2959–2973, doi:10.5194/bg-7-2959-2010, 2010.

931 Weijers, J. W. H., Steinmann, P., Hopmans, E. C., Schouten, S. and Sinninghe Damsté, J. S.:
932 Bacterial tetraether membrane lipids in peat and coal: Testing the MBT-CBT temperature
933 proxy for climate reconstruction, *Organic Geochemistry*, 42(5), 477–486,
934 doi:10.1016/j.orggeochem.2011.03.013, 2011.

935 Xie, S., Pancost, R. D., Chen, L., Evershed, R. P., Yang, H., Zhang, K., Huang, J. and Xu, Y.:
936 Microbial lipid records of highly alkaline deposits and enhanced aridity associated with
937 significant uplift of the Tibetan Plateau in the Late Miocene, *Geology*, 40(4), 291–294,
938 doi:10.1130/G32570.1, 2012.

939 Zech, M. and Glaser, B.: Compound-specific $\delta^{18}\text{O}$ analyses of neutral sugars in soils using gas
940 chromatography-pyrolysis-isotope ratio mass spectrometry: problems, possible solutions
941 and a first application, *Rapid Communications in Mass Spectrometry*, 23, 3522–3532,
942 doi:10.1002/rcm, 2009.

943 Zech, M., Rass, S., Buggle, B., Löscher, M. and Zöller, L.: Reconstruction of the late
944 Quaternary paleoenvironments of the Nussloch loess paleosol sequence, Germany, using
945 n-alkane biomarkers, Quaternary Research, 78(2), 226–235,
946 doi:10.1016/j.yqres.2012.05.006, 2012a.

947 Zech, M., Kreutzer, S., Goslar, T., Meszner, S., Krause, T., Faust, D. and Fuchs, M.: Technical
948 Note: *n*-Alkane lipid biomarkers in loess: post-sedimentary or syn-sedimentary?,
949 Discussions, Biogeosciences, 9, 9875–9896, doi:10.5194/bgd-9-9875-2012, 2012b.

950 Zech, M., Tuthorn, M., Detsch, F., Rozanski, K., Zech, R., Zöller, L., Zech, W. and Glaser, B.:
951 A 220 ka terrestrial $\delta^{18}\text{O}$ and deuterium excess biomarker record from an eolian
952 permafrost paleosol sequence, NE-Siberia, Chemical Geology,
953 doi:10.1016/j.chemgeo.2013.10.023, 2013.

954 Zech, M., Mayr, C., Tuthorn, M., Leiber-Sauheitl, K. and Glaser, B.: Reply to the comment of
955 Sternberg on “Zech et al. (2014) Oxygen isotope ratios ($^{18}\text{O}/^{16}\text{O}$) of hemicellulose-
956 derived sugar biomarkers in plants, soils and sediments as paleoclimate proxy I: Insight
957 from a climate chamber experiment. GCA, Geochimica et Cosmochimica Acta, 141(0),
958 680–682, doi:10.1016/j.gca.2014.04.051, 2014.

959 Zech, M., Zech, R., Rozanski, K., Gleixner, G. and Zech, W.: Do *n*-alkane biomarkers in
960 soils/sediments reflect the $\delta^2\text{H}$ isotopic composition of precipitation? A case study from
961 Mt. Kilimanjaro and implications for paleoaltimetry and paleoclimate research, Isotopes
962 in Environmental and Health Studies, 51(4), 508–524,
963 doi:10.1080/10256016.2015.1058790, 2015.

964 Zech, R., Gao, L., Tarozo, R. and Huang, Y.: Branched glycerol dialkyl glycerol tetraethers in
965 Pleistocene loess-paleosol sequences: Three case studies, Organic Geochemistry, 53, 38–
966 44, doi:10.1016/j.orggeochem.2012.09.005, 2012c.

967